Mineralium Deposita

The role of evaporites in the formation of gems during metamorphism of carbonate platforms: a review

--Manuscript Draft--

Manuscript Number:	
Full Title:	The role of evaporites in the formation of gems during metamorphism of carbonate platforms: a review
Article Type:	Regular Articles
Corresponding Author:	Gaston Giuliani, PhD. CRPG/CNRS Vandoeuvre, Meurthe et Moselle FRANCE
Corresponding Author Secondary Information:	
Corresponding Author's Institution:	CRPG/CNRS
Corresponding Author's Secondary Institution:	
First Author:	Gaston Giuliani, PhD.
First Author Secondary Information:	
Order of Authors:	Gaston Giuliani, PhD.
	jean Dubessy, PhD.
	Daniel Ohnenstetter, PhD.
	David Banks, PhD.
	Yannick Branquet, PhD.
	Julien Feneyrol, PhD.
	Anthony Fallick, PhD.
	Jean-Emmanuel Martelat, PhD.
Order of Authors Secondary Information:	
Funding Information:	Département Soutien et Formation, Institut de Recherche pour le Développement — Dr. Gaston Giuliani
Abstract:	The mineral and fluid inclusions trapped by gemstones during the metamorphism of rocks in carbonate platform successions are precious markers for the understanding of the gem genesis. The nature and chemical composition of inclusions highlight the major contribution of evaporites through dissolution or fusion, depending on the temperature of formation from the greenschist to the granulite facies. The fluids are highly saline NaCl-brines circulating either in an open system in the greenschist facies (Colombian and Afghan emeralds) and with huge fluid-rock metasomatic interactions, or sulphurous fluids (ruby, garnet tsavorite, zoisite tanzanite and lapis-lazuli) or molten salts formed in a closed system with a low fluid mobility (ruby in marble) in the conditions of the amphibolite to granulite facies. These chloride-fluoride-sulphate ± carbonate-rich fluids scavenged the metals essential for the gem formation. At high temperature, anions SO42-, NO3-, BO3- and F- which are powerful fluxes lowered the temperature of chlorine and fluoride ionic liquids. They provided transport over a very short distance of aluminium, and/or silica and transition metals which are necessary for gem growth. So, the genetic models proposed for these high-value and ornamental gems underline the importance of the metamorphism of evaporites formed on carbonate continental shelves, and emphasises the chemical power accompanying the metamorphism at moderate to high temperatures of these particular evaporite-rich and organic matter-rich protoliths to form gem minerals.
Suggested Reviewers:	Bernd Lehmann, PhD.

	Editor Mineralium Deposita, Technical University of Clasthal lehmann@min.tu-clausthal.de Dr. Bernd Lehmann, Editor of Mineralium Deposita, who invited us to write this paper on the role of evaporites in the formation of metamorphic gems, published in a short version as "Le fluide, l'Arlésienne du métamorphisme" in the Journal Géochronique, N°136, décembre 2015 entitled "Regards croisés sur le métamorphisme".
	Georges beaudoin, PhD. professor, Universite Laval Georges.Beaudoin@ggl.ulaval.ca As an Editor of Mineralium Deposita, Journal who invites our group to submit the present ms. Dr. Beaudoin participated to the bank of PhD. theis of Julien Feneyrol one of the authors.He knows well the gem thematic
	Robert Linnen, PhD. Professor, Western University r.linnen@uwo.ca geochemist specialist of fluids who has experience and knowledge in gems formation

The role of evaporites in the formation of gems during metamorphism of carbonate platforms: a review

Gaston Giuliani[1,2], Jean Dubessy[3], Daniel Ohnenstetter[4], David Banks[5], Yannick Branquet[6,7], Julien Feneyrol[8], Anthony E. Fallick[9], Jean-Emmanuel Martelat[10]

1- Université Paul Sabatier, GET/IRD, UMR CNRS-IRD-CNES 5563, 14 avenue Edouard Belin, 31400 Toulouse, France
2- Université de Lorraine, CRPG UMR 7358 CNRS-UL, 15 rue Notre-Dame-des-Pauvres, BP 20, 54501 Vandœuvre-lès-Nancy cedex, France
3- Université de Lorraine, GeoRessources UMR 7359 CNRS-UL, BP 70239, 54506 Vandœuvre-lès-Nancy, France
4- 4 rue Nicolas Chopin, 88130 Marainville-sur-Madon, France
5- University of Leeds, School of Earth and Environment, Woodhouse Lane, Leeds LS2 9JT, United Kingdom
6- ISTO, UMR 7327-CNRS/Université d'Orléans/BRGM, 1A rue de la Férollerie, 45071 Orléans cedex 2, France
7- Géosciences-Rennes, UMR6881-CNRS/Université de Rennes I, Campus de Beaulieu, 35042 Rennes Cedex, France
8- Arethuse Geology, Latitude Arbois, 1060 Rue René Descartes, 13290 Les Milles, France
9- Isotope Geosciences Unit, S.U.E.R.C., Rankine Avenue, East Kilbride, Glasgow G75 0QF, Scotland, United Kingdom
10- Laboratoire de Géologie de Lyon (LGLTPE), Université de Lyon 1, ENSL, UMR 5276, 2 rue Raphaël Dubois, Géode, 69622 Villeurbanne Cedex, France

Abstract The mineral and fluid inclusions trapped by gemstones during the metamorphism of rocks in carbonate platform successions are precious markers for the understanding of the gem genesis. The nature and chemical composition of inclusions highlight the major contribution of evaporites through dissolution or fusion, depending on the temperature of formation from the greenschist to the granulite facies. The fluids are highly saline NaCl-brines circulating either in an open system in the greenschist facies (Colombian and Afghan emeralds) and with huge fluid-rock metasomatic interactions, or sulphurous fluids (ruby, garnet tsavorite, zoisite tanzanite and lapis-lazuli) or molten salts formed in a closed system with a low fluid mobility (ruby in marble) in the conditions of the amphibolite to granulite facies. These chloride-fluoride-sulphate ± carbonate-rich fluids scavenged the metals essential for the gem formation. At high temperature, anions SO_4^{2-}, NO_3^-, BO_3^- and F^- which are powerful fluxes lowered the temperature of chlorine and fluoride ionic liquids. They provided transport over a very short distance of aluminium, and/or silica and transition metals which are necessary for gem growth. So, the genetic models proposed for these high-value and ornamental gems underline the importance of the metamorphism of evaporites formed on carbonate continental shelves, and emphasises the chemical power accompanying the metamorphism at moderate to high temperatures of these particular evaporite-rich and organic matter-rich protoliths to form gem minerals.

Keywords

gems, emerald, ruby, garnet, zoisite, lapis-lazuli, metamorphism, carbonate platform, evaporites, brines, fingerprints, salinity, molten salts, thermal reduction of sulphates

Introduction

The classical quality-grading criteria for gems are based on clarity, colour, carat and cut. These 4 "C" criteria are dependent on the geological, physical and chemical conditions existing during the gem growth. The formation of coloured gems necessitates the existence of four conditions: (1) a parental fluid issued either from the gem host-rock environment or exotic fluid circulations; (2) a seed surface and sufficient space for the growth of the crystal; (3) the incorporation of trace elements from the parental fluid in the unit cell of the mineral; and (4) the absence of internal crystalline deformation during and after growth.

The colour and transparency will make the difference between a mineralogical specimen and a gem. The chromophores are mostly transition metals such as Ti, V, Cr, Mn, Fe, Cu which have approximately the same atomic radius as the substituted major element(s) of the mineral. On the other hand, the exceptional optical quality of gemstones make them an object of choice for the study of solid and fluid inclusions (FI) trapped during their growth, and these are sometimes excellent geological and/or geographical fingerprints (Giuliani et al. 2014a).

This paper is focused on metamorphic gems and ornamental gemstones such as Colombian and Afghan emeralds, ruby-bearing marbles in central and south-east Asia, garnet vanadium-rich grossular i.e. tsavorite and vanadium-rich zoisite called tanzanite from Tanzania, Kenya and Madagascar, and lapis-lazuli in marble and/or calc-silicate rocks from Afghanistan (Fig. 1). Previous studies highlighted special common features: (i) the presence of halite, sulphates and minerals rich in Cl, Na, Mg, B and F; and (ii) either the trapping of high-salinity aqueous (± carbonic) FI or CO_2-H_2S-S_8-rich FI (Roedder 1963; Giuliani et al. 1993a; Giuliani et al. 2003; Garnier et al. 2008; Feneyrol et al. 2013; Giuliani et al. 2015a). Three questions arise concerning these metamorphic gems primarily due to change in the conditions of heat and pressure, and fluid-rock interactions by diffusion or percolation (metasomatism): (1) the origin and the role of these fluids; (2) the nature and the importance of the protolith; and (3) the characteristics of the paleogeography of the depositional sedimentary environment. During this review, we will show the efficiency of different analytical techniques which allow the acquisition of relevant data for answering these questions.

The geological setting of metamorphic gems

Recent petrographical and geochemical data obtained on the formation of metamorphic deposits such as Colombian and Afghan emeralds, Asian ruby-bearing marbles, tsavorite and tanzanite in East Africa (Groat 2014), and lapis-lazuli of Sar-e-Sang in Afghanistan (Faryad 2002), allowed the characterization of the protoliths of these gem-bearing metamorphic rocks. These are calcareous benches alternating with black shales (BS), initially rich in organic matter (OM), with intercalation of levels of evaporitic rocks. The latter are not recognizable after metamorphism as such, but mineralogy and paleofluids contained in primary fluid inclusions witness their past presence (Giuliani et al. 2003).

Colombian emerald deposits

Located in the Eastern Cordillera basin, the Colombian emerald deposits define two belts: the eastern belt encompassing the mining districts of Gachalá, Chivor and Macanal, and the western belt including the mining districts of Yacopi, Muzo, Coscuez, La Pita and Peñas Blancas (Fig. 2A). Emerald mineralisation is hosted in the Lower Cretaceous sedimentary series characterized by a succession of sandstone, limestone, black shale (BS), and evaporites (Fig. 3). Detailed structural mapping and geometric analysis provided evidence that emerald mineralisation is associated to structural events drastically different between the western and eastern belts (Branquet et al. 1999a). The Muzo and Coscuez deposits are linked to tear faults and associated thrusts during a compressive tectonic event whereas the eastern emerald deposits, such as that of Chivor, present extensional structures extending from a brecciated evaporitic level which acted as a local, gravity-driven detachment. These tectonic structures are both synchronous with the circulation of hydrothermal fluids and emerald formation. The fluid-rock interaction processes led to Na and Ca metasomatism of the enclosing carbonated carbon-rich BS. Leaching of major (K, Al, Si, Ti, Mg, P), trace (Be, Cr, V, Rb, Sc, U, C) and REE elements from the BS is accompanied by their partial redistribution to minerals in the in-filling vein system, especially Cr and V which are incorporated in emerald (Giuliani et al. 1993b). Emerald formed at a temperature (T) ~ 300-330°C and a pressure (P) ~ 0.5-1.2 kbar which correspond to a depth about 4 to 5 km (Cheilletz et al. 1994; Ottaway et al. 1994).

The eastern emerald belt: the Chivor mines

The mines are scattered along a regional white-brecciated evaporitic unit which contains emerald veins (Fig. 2B). The brecciated rock unit in the Chivor area, which is in excess of 10 km long and 10 m thick (Figs. 4A, B), is stratiform, i.e. parallel to the sedimentary strata, and dominantly composed of a breccia (Fig. 4C) made up of fragments from the hanging wall

(carbonated carbon-rich BS, limestone and whitish albitite, i.e. an albitised BS) cemented by carbonates and pyrite (Fig. 4D). Its formation is related to the dissolution of an evaporitic horizon (Branquet et al. 2015). All the mineralized structures extend vertically from the brecciated level. In the Chivor mines, emerald is located in cm- to dm-thick carbonate-pyrite–bearing (Fig. 1A) listric faults, meter-wide extensional fractures injected with hydrothermal breccia, and extensional sets of fractures in the albitite (Fig. 4E) and calcareous carbon-rich BS of the Macanal Formation. The brecciated level, the hydrothermal fluid circulation and emerald formation occurred at 65 ± 3Ma (Cheilletz et al. 1997).

The western emerald zone: the Muzo and Coscuez mining districts

On the western side, the deposits are hectometer-sized at most and display numerous folds, thrusts and tear faults (Fig. 5; Laumonier et al. 1996; Branquet et al. 1999a). At the Muzo deposit, thrusts are characterized by the carbonated BS which overlie siliceous BS (Fig. 6). All the tectonic contacts are marked by cm- to m-thick hydrothermal breccias called by the local miners "cenicero", i.e. ashtray (generally, well delimited white coloured zone which has the aspect of ash during the dry season). These white- or red-coloured breccias outline the thrust planes, which are associated with intense hydraulic fracturing (Branquet et al. 1999b). Multistage brecciation corresponds to successive fault-fluid flow pulses, and dilatant sites resulting from shear-fracturing synchronous to the thrust fault propagation. Each pulse is associated with: (i) emerald-bearing banded carbonate vein-like structures present throughout the breccia; (ii) emerald-bearing thrust-associated carbonate veins occurring in the wall rocks and composed of calcareous BS called "cama" by the local miners (emerald zone forming a layer which is parallel to the thrust fault); and (iii) emerald-bearing carbonate veins initiating in the breccia zone and crosscutting the wall-rocks. All of these tectonic structures are associated with fluid circulation in the calcareous carbon-rich BS which induced intense albitisation, carbonatisation and pyritisation. The siliceous BS called "cambiado"(zones which have changed by comparison with the cama) by the local miners have no mineralisation.

At the Coscuez deposit, the folds and thrusts were guided by the Coscuez tear fault which acted as a vertical conduit for the mineralizing fluids developed in the carbonated carbon-rich BS. Hydraulic breccias (Fig. 7), formed by the opening of dilatant sites related to fluid over-pressures and hydrothermal replacement, are similar to those described for the Muzo deposit. The genesis of the deposit is the consequence of a compressive phase characterized by folding and thrusting along tear faults formed at the Eocene-Oligocene boundary (Cheilletz et al. 1994) and associated with fluid overpressure. These complex structures are probably linked to

a basal regional décollement or detachment fault thought to be at the level of the evaporites (Branquet et al. 1999a, b).

At the regional scale, the presence of sedimentary levels with gypsum, residues of dissolution of salts (called "rute" by Colombian miners) in the Lower Cretaceous series of the Eastern Cordillera and saliferous diapirs, confirm that the continental shelf series is saliferous. The significant albitisation of the BS and precipitation of albite in the hydrothermal veins (Branquet et al. 1999a) testifies to important brine circulations. Furthermore, at the Chivor mines, the presence in the upper albitites (see Fig. 4A) of coalescent replacement of anhydrite nodules into carbonates, tepee and enterolithic structures argue for the evaporitic origin of the protolith (Branquet et al. 2015).

Emerald deposits from Afghanistan

The main commercial emerald deposits are centred on the Panjshir Valley, 230 km NW of Kohistan (Bowersox et al. 1991; Fig. 8). The valley coincides with the Herat-Panjshir strike-slip fault which was active in the Oligo-Miocene (Tapponnier et al. 1981). The emerald deposits, located on the southeastern part of the Panjshir fault zone, are dated, by Ar-Ar technique on micas, at 23 ± 1 Ma (Sabot et al. 2000). The Kendjt, Khalat and Gujari deposits are located along the shear zone cutting Palaeozoic metasedimentary rocks formed by intercalations of schist, dolomitic marble and quartzite, in the upper greenschist facies (Kazmi and Snee 1989; Vapnik and Moroz 2001). Emerald is confined to quartz-ankerite-dolomite-pyrite veinlets and veins linked to shear zones (Fig. 1C). The metasomatic alteration due to the fluid circulation resulted in the phlogopitisation, albitisation and silicification of the wall-rocks. Albitites resembling those of Colombia are described by Sabot et al. (2000). The metasomatic minerals include dravite tourmaline, pyrite, albite and phlogopite. The origin of chromium, vanadium and beryllium is unknown because there are no reported whole-rock analysis of the emerald-hosting metamorphic formations.

Ruby and lapis-lazuli from central and south-east Asia

Ruby in marble deposits

One of the main worldwide sources for excellent-quality ruby with intense colour and high transparency (Fig. 1D) is associated with marble deposits from central and south-east Asia (Hughes 1997). The deposits occur in Afghanistan, Pakistan, Azad-Kashmir, Tajikistan, Nepal, Myanmar, northern Vietnam and southern China (Garnier et al. 2008; Fig. 8). These

deposits are found in metamorphosed platform carbonates associated generally with marbles intercalated with garnet-biotite-sillimanite- or biotite-kyanite-bearing gneisses which are sometimes intruded by granitoids (Pêcher et al. 2002). The marble units consist of discontinuous horizons up to 300 m in thickness, oriented parallel to the main regional foliations, thrusts or shear zones related to the Cenozoic Himalayan orogenesis between 45 and 5 Ma (Garnier et al. 2006). The ruby mineralisation is restricted to peculiar impure marble horizons. The protolith of the ruby-bearing metamorphic rocks comprises carbonates enriched in detrital clays and organic matter (OM), and intercalated evaporitic layers (Fig. 3). Ruby crystals occur: (i) disseminated within marbles and associated with phlogopite, muscovite, scapolite, margarite, spinel, titanite, pyrite and graphite, as in Jegdalek, Afghanistan; Chumar and Ruyil, Nepal; Hunza and Nangimali, Pakistan; Mogok and Mong Hsu, Myanmar; and Luc Yen, Vietnam; (ii) in veinlets or gash veins, as in some occurrences in northern Vietnam, and associated with phlogopite, margarite, titanite, graphite and pyrite, and sometimes related to micro-shear zones, as in Nangimali in Pakistan; (iii) in pockets associated with orthoclase, phlogopite, margarite, graphite and pyrite in some occurrences of northern Vietnam. Gem ruby formed during the retrograde metamorphism stage at T ~ 620-670°C and P ~ 2.6-3.3 kbar (Garnier et al. 2008). The aluminium and the chromophorous elements of ruby originate from the marbles (Al up to 1000 ppm, V and Cr between 5 to 30 ppm).

Lapis-lazuli deposits

The antique and famous ornamental lapis-lazuli deposits at Sar-e-Sang in the north-eastern part of Afghanistan (Fig. 8) occur within the high-grade metamorphic rocks of the Goran series. U-Pb, K-Ar and Rb-Sr radiometric data gave a minimum Proterozoic age at 2.13 Ga for the amphibolite facies metamorphism of the Goran series (Russian literature cited in Hubbard et al. 1999) while $^{40}Ar/^{39}Ar$ ages of micas associated with micaschist and phlogopite from ultramagnesian rocks gave a range of ages, from 17 to 22 Ma, indicative of a Miocene cooling age due to Himalayan exhumation activity (Hubbard et al. 1999). The lapis-lazuli formed lenses or layers in calcite and dolomite marbles containing fine lenses or more thicker anhydrite levels (Kulke 1974) and white schists (Kulke and Schreyer 1973) intercalated with calc-silicate rocks, amphibolites and quartzites, and occur also at the contact between granite or pegmatite with marble (Faryad 2002). The thickness of the lenses and layers is between 2 to 6 m while the extension is between 40 to 450 m. Generally, the central part of the layers formed by calcite-diopside-lazurite (Fig. 1F) is bordered, on one side, by a diopside-rich zone

(40 to 90 vol. %), and on the other side by a phlogopite-diopside-calc-silicate rock zone (with also scapolite, tremolite, zoisite, epidote). P-T conditions of metamorphism are T ~ 750°C and P ~ 13-14 kbar (Faryad 2002).

Garnet tsavorite and zoisite tanzanite in East Africa

All tsavorite deposits are hosted in the Neoproterozoic Metamorphic Mozambique Belt (NMMB) stretching from the Arabian-Nubian shield to East Antarctica, through East Africa, Madagascar and Pakistan (Feneyrol et al. 2013). The economic deposits are found in Kenya, Tanzania and Madagascar (Fig. 9). They formed during Neoproterozoic Himalayan-type continental collision between eastern and western Gondwana blocks, between 650 and 550 Ma, following the complex closure of the Mozambique Ocean. Tsavorite is hosted by a metasedimentary sequence (Fig. 3) formed by a succession of quartzite, kyanite ± sillimanite-biotite ± almandine graphitic gneiss, graphitic gneiss with intercalations of calc-silicate rock, meta-evaporite and marble (Olivier 2006; Feneyrol et al. 2010). The calc-silicate rocks in the graphitic gneisses display enterolithic structures (Figs. 10B, C) and ± anhydrite-diopside and tsavorite nodules (Figs. 10A, D; Feneyrol et al. 2013).

Tsavorite is mined within primary deposits either as nodules (Type I) or in quartz veins (Type II), and placers (Type III):

(i) *Type I:* the nodules (Fig. 1E) and meta-evaporite levels are stratiform and occur among calc-silicates and graphitic gneisses such as in the Kenyan tsavorite belt (Fig. 9C; Fig. 10A). The tsavorite-bearing nodules are scattered in the Ca-rich rocks and formed through metamorphic reactions between calcareous beds or concretionary lenses and sulphate-rich levels intercalated within carbon-rich shale (Fig. 10A). The nodules formed during prograde metamorphism and tsavorite formed upon anhydrite or barite at T ~ 580-690°C and P ~ 5-7 kbar (Feneyrol et al. 2013).

In the deposits from Kenya, Tanzania and Madagascar, V and Cr contents of graphitic gneisses are respectively up to 3600 ppm and 900 ppm (Fig. 3). In Tanzania, for the Merelani deposit (Fig. 9C), the source of V for tsavorite is apparently graphite hosted by the graphitic gneiss, which has a V content up to 2600 ppm indicating that original OM was V-rich (Olivier 2006). In the Lemshuku deposit (Fig. 9C), the graphite associated with the gneiss and calc-silicate rocks has no V and Cr but the V and Cr contents of the graphite-bearing gneisses are respectively, between 200 and 2000 ppm, and 60 and 300 ppm (Feneyrol 2012). The V and Cr precursors have been consumed during the prograde metamorphism to form V and Cr-bearing kyanite, graphite, muscovite, rutile, diopside, titanite or karelianite.

(ii) *Type II:* deformation played an important role in the mineralizing processes for the quartz vein deposits found in Tanzania (Merelani and Ruangwa deposits; Figs. 9A, C). Vein formation and hydrothermal-metasomatic fluid circulation (carbonatisation, pyritisation and graphitisation) affecting the graphitic gneisses and calc-silicates were coeval with regional metamorphism (Feneyrol et al. 2013). Tsavorite in veins and pockets (Fig. 1G) formed during the retrograde stage at T 505-590°C and P ~ 3.6-4.9 kbar. Gem tanzanite at Merelani (Fig. 1H) formed later in pockets and lenses at T ~ 385-450°C and P ~ 2.2 and 3.6 kbar (Feneyrol 2012). It is associated with low grade metamorphic assemblages with commonly prehnite, (± quartz) and calcium zeolites (chabazite, heulandite, mesolite, laumontite), axinite and blue apatite (Wilson et al. 2009).

In conclusion, gems mentioned in this study formed during the metamorphism of sedimentary carbonate platform formations containing evaporitic rocks from Neoproterozoic to Cenozoic time, and at temperatures between 300 and 750°C. The question arises as to the nature of the gem protolith and the geochemistry of the fluids. In the next section, we will focus on detailed aspects showing the importance of evaporites in the formation of these gems and their associated paragenesis.

The mineral and geochemical fingerprints of the past presence of evaporites

Mineralogy

In the Colombian deposits, crystals of anhydrite, halite and sometimes sylvite are trapped by emerald, quartz, albite and pyrite (Giuliani et al. 1993a).

In the ruby deposits, variations of local chemistry of the protolith along several decimetres are due to lateral facies variations which resulted in a succession of different paragenesis: (1) F-aspidolite (sodic phlogopite with Na_2O between 6.2 and 6.6 wt. %, K_2O between 0.4 and 0.6 wt. %, and MgO between 25.8 and 26 wt. %) associated with F-phlogopite and F-paragonite in the different mineralized zones of ruby, as evidenced in the Nangimali deposit in Pakistan (Garnier et al. 2004); (2) anhydrite either associated with F-tremolite, - edenite, - pargasite, and calcite in samples from the Hunza Valley, Pakistan, and Luc Yen, Vietnam, or included in ruby with relics of spinel (Fig. 11A); (3) anhydrite and salt crystals ($CaCl_2$, NaCl and KCl) as solid inclusions (Figs. 11C to E) in most of the rubies observed by SEM method, as in

Nangimali and Luc Yen deposits (Garnier et al. 2008), and (4) F-bearing minerals such as dravite-uvite tourmaline and apatite indicating a low activity of water in the fluid.

In the tsavorite and tanzanite deposits, the presence of different metamorphic mineral associations results from lateral facies variations of the initial protolith. Tsavorite from the deposit of Namalulu in Tanzania, is associated with F-Na-Cl-SO_4-Li-rich minerals that indicate the presence of rich precursor evaporite-bearing sediments in the protolith (Feneyrol et al. 2012): (i) the Na-Ca-Cl-scapolites with Na_2O between 6.5 and 7.9 wt. % and Cl between 2.3 and 2.8 wt. % as well as F-tremolite (F up to 3.8 wt. %); (ii) anhydrite crystals associated with F-tremolite and dolomite in lenses in dolomitic marble (Fig. 11F); (iii) F-rich titanite with very high F-content (1 to 1.6 wt. % F) as well as phlogopite (2 to 4.8 wt. % F); (iv) the nodules of tsavorite concentrate towards their periphery F-bearing minerals with high F^-/OH^- ratio such as F-phlogopite (Fig. 10D) and F-apatite, testifying again to a low activity of water in the fluid and a strong fluoride activity; and (v) tsavorite is associated with a rare mineral described for the first time in the metamorphic environment (Feneyrol et al. 2012): the F-tainiolite (Fig. 11G) {$KLiMg_2(Si_4O_{10})(F,OH)$} which contains 8.9 to 9.4 wt. % F, 2 wt. % LiO_2, and between 50 and 110 ppm of boron. Tainiolite is associated with a F-tremolite containing 3.5 wt. % F and up to 730 ppm of lithium. Additionally, barite is observed in the nodules of tsavorite at the Nadan 1 mine in Kenya (Fig. 11B).

At Sar-e-Sang lapis-lazuli deposit, scapolite and halogen-bearing minerals formed during prograde metamorphism of carbonate-evaporite sequences: (i) scapolite with Na_2O between 3.8 and 12.4 wt. % and Cl between 0.3 and 4.2 wt. %; (ii) sodalite close to the ideal end-member $Na_4Al_6Si_6O_{12}Cl$; (iii) haüyne and lazurite with compositions respectively, $Ca_{1.2}Al_6Si_6Cl_{0.2}O_{29}$ and $Na_{5.5}Ca_{0.9}Al_{5.8}Si_6Cl_{0.1}O_{29}$; (iv) F-phlogopite (F ~ 1 to 3.4 wt. %); (v) Na-amphibole (F-Cl-pargasite and edenite with Cl ~ 1.1 and 1.7 wt. % Cl); (vi) F-Cl-apatite containing chlorine up to 6.8 wt% and fluorine up to 4.8 wt. % (Faryad 2002). The presence of Na-Cl-scapolite implies an evaporitic source with NaCl provided by salt-rich layers (Faryad 2002). Besides, the magnesian kyanite-sillimanite-cordierite-dravite talcschists associated with these lazurite-bearing marbles result also from the metamorphism of evaporites (Schreyer and Abraham 1976). The dravite contains around 2.6 wt. % Na_2O and 0.1 to 0.13 wt. % F.

In conclusion, all these gemstones contain F (excepted Colombian emeralds), Cl, Li, Na, Mg and B mineralogical markers which testify to the importance played by the intercalations of

334 evaporitic levels in the sedimentary series which were subsequently metamorphosed during
335 orogenesis. For the Colombian emeralds, the circulation of chlorine and sodium brines in the
336 décollement zones of the basin, responsible for the albitisation of the BS coeval with emerald
337 formation, characterised the end of the subsidence of the basin which was associated with the
338 first tectonic-metamorphic episode affecting the eastern border of the Eastern Cordillera
339 basin. The second tectonic phase reactivated similar fluid circulation processes on the western
340 border. In both borders, the process for crystallisation of emerald took place in an open
341 hydrothermal-metamorphic system. In Afghanistan, the absence of detailed geology and
342 petrography of the deposits precludes any comprehensive genetic hypothesis, but the emerald
343 veins are related to shear zones and fluid circulation led to the albitisation of the schists.
344 For the other gems, the marbles or the gneisses contained intercalations of calc-silicate rocks
345 and meta-evaporites. The chemical reactions are strongly spatially limited to the nodules
346 and/or to the lenses of evaporites, which is evidence of a very low fluid circulation. The
347 formation of ruby, tsavorite, tanzanite and lapis-lazuli occurred in quasi-closed systems.
348
349 **Geochemistry of the paleo-fluids**
350 Paleo-fluids trapped as primary FI in the minerals during their growth allow accession to the
351 composition of the mineralising fluids. Different techniques are used for their characterisation
352 such as microthermometry, Raman and infrared spectrometries, crushing of FI for analysis of
353 the cations and anions, and analysis of noble gases (Samson et al. 2003). The combination of
354 these data with those obtained on the stable isotope ratios of elements such as oxygen,
355 hydrogen, sulphur and boron on minerals coeval with the gems, permits the characterization
356 of the origin and source of the different chemical elements.

357 *Colombian emerald*

358 Fluids trapped by emerald are commonly three-phase FI (Fig. 12A) characterized by the
359 presence of a daughter mineral, i.e. halite (NaCl). At room temperature, the cavities contain
360 75 vol. % of salty water, i.e. an aqueous brine (liquid H_2O), 10 vol. % of gas corresponding to
361 the vapour bubble (V), and 15 vol. % of halite daughter mineral (H). However, some
362 Colombian emeralds have multiphase FI presenting a liquid carbonic phase (CO_2) forming up
363 to 3 vol. % of the total cavity volume (Figs. 3A, 12B), minute crystals of calcite (Fig. 12A),
364 very rare liquid and gaseous hydrocarbons (Kozlowski et al. 1988), and sometimes two or
365 three cubes of halite (Figs. 12A, 12B), and sylvite (KCl). These H_2O-NaCl±CO_2-(Ca-K-Mg-
366 Fe-Li-SO_4) fluids (Banks et al. 2000) are NaCl saturated (~ 40 wt% eq. NaCl) and were

367 trapped at T ~ 300-330°C (Roedder 1963; Giuliani et al. 1993a; Cheilletz et al. 1994; Ottaway
368 et al. 1994). The high Cl/Br ratio of the fluids (between 6,300 and 18,900) indicates that the
369 strong salinity of the brines derived from dissolution of halite of evaporitic origin (Fig. 13A;
370 Banks et al. 2000). Cation exchanges, especially calcium, with the BS host rocks are strong
371 when compared to most basinal and bittern fluids (Yardley and Bodnar 2014) and due to the
372 relatively high temperature of the parent brines of emerald. Indeed, these fluids are enriched
373 in Ca (16,000 to 32,000 ppm), base metals (Fe ~5,000 to 11,000 ppm; Pb ~125-230 ppm; Zn
374 ~170-360 ppm), lithium (Li~400-4300 ppm) and sulphates (SO_4 ~400-500 ppm).
375 Nevertheless there is no fluorine in these fluids (Table 1). As comparison, they have a
376 composition and Fe/Cl and Cl/Br ratio (Table 1) similar to the fluids of the geothermal system
377 of Salton Sea in California (Fig. 13B; Yardley and Cleverley 2013). The K/Na ratios confirm
378 the Na-rich character of the fluids and the strong disequilibrium between K-feldspar and
379 albite, as illustrated by the huge albitisation of the BS (Fig. 14).
380 The isotopic composition of the oxygen ($\delta^{18}O$) of H_2O in equilibrium with Colombian
381 emerald, calculated at 300°C, are higher ($15.5 < \delta^{18}O < 17.1$ ‰ for the eastern belt, and 17.5
382 $< \delta^{18}O < 23.6$ ‰ for the western belt; Giuliani et al. 2000) than those of classical basinal
383 waters which have lower temperatures of formation. Besides, the range of values of isotopic
384 composition of sulphur ($\delta^{34}S$) of pyrite associated with emerald (Fig. 1A) corresponds to the
385 isotopic range of values for sulphates (marine anhydrite) of the Lower Cretaceous of
386 Colombia (Giuliani et al. 1995).

387 *Afghan emerald*

388 Primary multiphase halite-sylvite-bearing FI (Fig. 12C) are common for the Panjshir emeralds
389 (Kazmi and Snee 1989; Giuliani et al. 1997). The fluids associated with emerald precipitation
390 have total dissolved salts (TDS) between 300 and 370 g/l and the trapping temperature of the
391 fluid is about 400°C (Vapnik and Moroz 2001).
392 Crush-leach analyses of the electrolyte chemistry of fluid inclusions are presented in Table
393 1. The fluids are Cl-Na-rich and they contain sulphates ($140 < SO_4 < 4,300$ ppm) and lithium
394 ($170 < Li < 260$ ppm) but very low to zero fluorine contents (Table 1). The K/Na ratio of the
395 fluid inclusions confirms the disequilibrium, at ~ 400°C, between K-feldspar and albite which
396 drives the Na-metasomatism of the metamorphic schists and the deposition of albite in the
397 veins (Fig. 14). Crushing demonstrates that fluids are dominated by NaCl with Cl/Br ratios
398 much greater than that of seawater (Fig. 13A), indicating that the salinity was derived by
399 dissolution of halite. Thus the high Cl/Br ratios are consistent with halite dissolution for the

origin of salinity. The diagram I/Cl versus Br/Cl (Fig. 13B) shows also that the fluid inclusions have low I contents that are also typical of brines derived from evaporite dissolution. They compare with Hansonburg and contemporary fluids from the Salton Sea geothermal brines (Fig. 13B), both of which have dissolved evaporites (Williams and McKibben 1989; Bolkhe and Irwin 1992).

Ruby in marble

Microthermometry studies combined with Raman spectroscopy of primary FI trapped by ruby indicate the contemporary trapping of two types of carbonic FI (Giuliani et al. 2015a): mono- to two-phase FI (Fig. 3) in the system CO_2-H_2S-($\pm$ COS $\pm$ S_8) $\pm$ (H_2O, $<$ 10 mol. %) and polycrystalline FI (Fig. 12D) in the system (Na-K-Ca-CO_3-SO_4-NO_3-Cl-F) $\pm$ (CO_2-H_2S) $\pm$ (H_2O). The different solids in the polycrystalline FI are mixtures of carbonates with Ca-Na-Al cations, such as shortite and dawsonite, sulphates - mainly anhydrite and barite, phosphates (F-apatite), nitrates, fluorides (fluorite), and chlorides (halite, Ca and K chlorides). These solids are daughter minerals (Fig. 12D) of ionic liquids formed during the metamorphism of evaporites and limestones (Giuliani et al. 2015a). As comparison, the polycrystalline inclusions represent for ruby the product of crystallization of molten salts, while for granites they are interpreted as the products of crystallization of silicate melts. In ruby, these polycrystalline FI are rare because if the salts are not immediately trapped by the crystals they are removed due to their strong solubility in water-rich fluids.

Crushing and leaching of rubies (Giuliani et al. 2015a) have shown that chloride is the dominant anion (25 to 53 mol. %) followed by sulphate (2 to 36 mol. %), nitrate (2 to 17 mol. %) and fluoride (0 to 25 mol. %). Sodium is the dominant cation (16 to 42 mol. %). The Li contents are very low (0.3 to 9 mol. %). The presence of nitrate, detected by both Raman spectroscopy and crush-leach techniques, is a strong argument for a continental input to the original sediment as, generally, nitrate salts precipitate in closed basin playas or salars (Ericksen 1983). In addition, the isotopic variation of sulphur of the anhydrites included in ruby and marble defines two sets of $\delta^{34}S$ values: the first, between 27 and 23 ‰, for a marine anhydrite; the second, between 4.8 and 1.6‰, for a continental source (Garnier et al. 2008).

Tsavorite and Tanzanite

The primary FI trapped by both minerals belong to the H_2S-S_8 ($\pm$ N_2 $\pm$ CH_4) system (Fig. 12E). Crush-leach analyses of tsavorite have shown that sulphate is the dominant anion (up to 50 mol. %) while lithium is absent and fluoride is very low (0 to 4 mol. %; unpublished data). SIMS *in situ* analyses of dravite tourmaline associated with nodules of tsavorite from Kenya,

Tanzania and Madagascar (Fig. 15) showed similar isotopic compositions of $\delta^{11}B$ = -19.8 ± 1.2‰ (n= 7). The range of boron isotopic composition (-20 <$\delta^{11}B$ < -18.5 %; Giuliani et al. 2015b) clearly indicates continental evaporitic materials and confirms the genetic model proposed for the formation of tsavorite in the metasedimentary series of the NMMB (Feneyrol et al. 2013). The sediments were derived from an ancient platform in a widespread and shallow evaporite-bearing epireic platform with alternation of marine and non-marine seaways on the border of the Mozambican Ocean.

Lapis-lazuli

Up to now the observations on the paragenesis associated with lapis-lazuli have not revealed the presence of cavities of FI or polycrystalline inclusions. Different minerals formed during the prograde and retrograde metamorphic stages. At peak P-T metamorphism, the presence of scapolite with diopside, grossular, calcite and quartz implies high CO_2 and NaCl concentrations in the fluid phases (X_{CO2} = 0.03-0.15 and X_{NaCl} between 0.04 and 0.99; Faryad 2002). During the retrograde stage, lazurite precipitated with sodalite, haüyne, F^- or Cl^--rich apatite, amphibole, scapolite, clinohumite and sometimes biotite.

Discussion on the role of evaporites in the formation of metamorphic gems

Parental brines of Colombian emeralds are responsible for the albitisation of the BS. They are at the origin of the mobilisation, under the form of chlorine and fluoride complexes, of aluminium, beryllium (Wood 1992), chromium (Vasin et al. 2004), vanadium (Povolov et al. 2007) and iron present in the BS. Sulphates are very sensitive to the conditions of thermal reduction, and in the presence of OM, the sulphate is reduced to sulphide (Machel et al. 1995), and OM is oxidized to CO_2 and then transformed into HCO_3^-:

$$(CH_2O_2)_{2\,(OM)} + SO_4^{2-}{}_{(fluid)} \rightarrow C_{(pyrobitumen)} + 2HCO_3^-{}_{(fluid)} + H_2S_{(fluid)} \quad (1)$$

Products of this thermal reduction of sulphate in the presence of OM are involved in the formation of carbonates and sulphides (Giuliani et al. 2000):

$$HCO_3^-{}_{(fluid)} + Ca^{2+}{}_{(fluid)} \rightarrow CaCO_{3\,(calcite)} + H^+{}_{(fluid)} \quad (2)$$

$$2HCO_3^-{}_{(fluid)} + Ca^{2+}{}_{(fluid)} + Mg^{2+}{}_{(fluid)} \rightarrow CaMg(CO_3)_{2\,(dolomite)} + 2H^+{}_{(fluid)} \quad (3)$$

$$7H_2S_{(fluid)} + 4Fe^{2+}{}_{(fluid)} + SO_4^{2-}{}_{(fluid)} \dashrightarrow 4\,FeS_{2\,(pyrite)} + 4H_2O_{(fluid)} + 6H^+{}_{(fluid)} \quad (4)$$

In the case of ruby hosted in marble, these redox reactions are also proposed to explain the association of pyrite and calcite with ruby (Giuliani et al. 2003):

$$CaSO_{4(anhydrite)} + 3/2C_{(graphite)} \rightarrow S°_{(fluid)} + CaCO_{3(calcite)} + 1/2CO_{2(fluid)} \quad (5)$$

$$CaSO_{4(anhydrite)} + 2C_{(graphite)} + H_2O \rightarrow H_2S_{(fluid)} + CaCO_{3(calcite)} + CO_{2(fluid)} \quad (6)$$

$$CO_{2(fluid)} + H_2S_{(fluid)} \rightarrow COS_{(fluid)} + H_2O \quad (7)$$

These reactions explain : (i) the involvement of anhydrite in these reactions, i.e. the presence of anhydrite crystals included in ruby and in marble shows that the reaction progress was not achieved to completion; (ii) the formation of CO_2 by oxidation of organic matter under graphitisation and/or graphite; (iii) the formations of native sulphur (reaction 5); (iv) the consumption of H_2O (reaction 6); and (v) the formation of COS gas in the primary fluid (reaction 7), a rare component in geological fluids, that implies H_2O-poor fluids.

The presence of SO_4^{2-}, NO_3^-, CO_3^{2-}, BO_3^- and F^- decreased consequently the temperature of melting of halite and other salts, and allowed the formation of chlorine and fluorine-bearing ionic liquids. The fluorine of continental origin probably played an important role in the extraction of the aluminium present in the impurities (clays) of the impure limestone. For comparison, the fluorine and aluminate-rich flux method is used by industry for the production of Al by electrolysis due to the formation of AlF^{4-} complexes (e.g. Lacassagne et al. 2002). So, the existence of an ionic liquid trapped in the form of polycrystalline solids by the ruby explains the colour and clarity of the ruby by: (i) the mobilization of Al, Cr and V contained in the metamorphosed limestone (Al ~ 1 000 ppm, Cr and V ~5 to 30 ppm for the Nangimali deposit in Pakistan); and (ii) their incorporation in an isotropic and fluid environment allowing crystalline growth with a minimum of defects (Giuliani et al. 2015a).

For tsavorite and tanzanite, the presence of anhydrite or barite in the tsavorite-bearing nodules as well as H_2S-S_8-bearing FI in tsavorite points out the importance of halite and sulphates in the gem formation. The notable quantity of F^- and Cl^- in phlogopite, titanite and scapolite associated with tsavorite, suggests that these elements have played a leading role in the mobilization of Al, and of V and Cr-bearing phengites and organic matter included in the anhydrite during the prograde metamorphism (Figs. 16B, 16C; Olivier 2006; Feneyrol et al. 2013).

For lapis-lazuli, the reduction of sulphates (Faryad 2002), at T ~ 750°C and P ~ 13-14 kbar, in the upper amphibolite to granulite facies, played a key role in its formation since blue colour results from the absorption of visible light by the radical S^{3-} present in its structure (Reinen and Lindner 1999). The radical S^{3-} was highlighted recently experimentally in aqueous fluids (Pokrovski and Dubrovinsky 2011; Pokrovski and Dubessy 2014) and also those resulting

from the thermal reduction of sulphate (Truche et al. 2014). The evaporitic protolith associated with lapis-lazuli formed an almost anhydrous chemical system which suggests that the S^{3-} radical could be stable also in ionic liquids originating from the melting and thermal reduction of evaporites at high temperature.

The set of geological and geochemical data obtained on these different deposits confirms the presence in the protoliths of evaporites, of either continental or marine origin, which are considered as a key feature in the metamorphic model for these gems (Fig. 16). They would have formed during the metamorphism, from the greenschist to granulite facies, of carbonates interbedded with OM-bearing mudstones, and containing intercalations of sulphates-chlorides-nitrates-borates of impure evaporitic rocks. The lithological control of the mineralisation is essential. These particular sedimentary lithologies and the nature of the metamorphic piles permit the delineation of the paleogeography of the depositional sedimentary environment. The sedimentary landscape converged to an epeiric carbonate platform succession with a combination of saltern and evaporite mudflats of gypsum and anhydrite such as described by Warren (2006).

The separation of the pericontinental and epicontinental seaways implies the presence of a sedimentary or a tectonic barrier, and at times the shallow epeiric seaway was converted to saltern mudflat (sabkha) with continental inputs. The presence of carbonate or siliciclastic and/or evaporitic matrix in the rocks is indicative of sediment deposited in a continental zone which was temporarily flooded by the tides, such as proposed for ruby hosted in metasediments (Garnier et al. 2008). The marine coastal sabkha environment is characterized by the formation of gypsum and anhydrite crystals, and nodules typically with enterolithic and 'chicken-wire' textures confirming their formation in supratidal zones such as described for the Colombian BS series and the Tanzanian and Kenyan metamorphosed BS formations. The high concentration of graphite in some metamorphic levels in the Kenyan Neoproterozoic tsavorite belt may represent original microbial mats (Feneyrol et al. 2013).

Perspectives

In spite of their differences in chemical composition, crystallisation system, physical conditions of metamorphism (P-T), scale of fluid circulation and ages, these metamorphic gemstones have in common a geochemical history connected to the nature of their mother protoliths.

Their mineralogical, chemical and isotopic characteristics are witnesses of fluid-rock interactions in open or closed systems. The understanding of their geological formation is one of the keys for the identification of their origin. The mineral and fluid inclusions trapped by gems during the metamorphism of rocks in carbonate platform successions are precious markers for understanding the genesis of the gems. The nature and chemical composition of the inclusions highlight the major contribution of evaporites by dissolution (for Colombian and Afghan emeralds) or melting (for other gems), depending of their temperature of formation. Solubility experiments of these gems in chloride-fluoride ionic liquids should be done together with speciation studies of the different chemical components involved in these minerals in order to generate thermodynamic models of such metamorphic ionic liquids.

Other worldwide deposits such as lapis-lazuli in Myanmar, Russia and Baffin Island in Canada, emeralds from Davdar and Musakashi, respectively in China and Zambia, Precambrian sodalite from Bahia state in Brazil, lazulite in the Neoproterozoic Itremo quartzite from central Madagascar, now suggest investigation of the possible presence of evaporites in the formation of these high-value and ornamental gems. Guidelines for prospecting new gem deposits of metamorphosed carbonate platform-related areas worldwide include: (i) the lithological control of the mineralisation from an ancient platform evaporite environment with alternation of marine and non-marine seaways, i.e. a marine coastal sabkha-like environment; (ii) the presence of index minerals such as anhydrite, scapolite, aspidolite, and chloride-fluoride-sulphate ± carbonate-rich fluid inclusions which can decipher the major contribution of evaporites by their dissolution or fusion, depending of their temperature of formation.

Acknowledgements

The authors would like to thank Dr. Bernd Lehmann, Editor of Mineralium Deposita, who invited us to write this paper on the role of evaporites in the formation of metamorphic gems, published in a short version as "Le fluide, l'Arlésienne du métamorphisme" in the Journal Géochronique, N°136, décembre 2015 entitled "Regards croisés sur le métamorphisme".

References

Banks D, Giuliani G, Yardley BWD, Cheilletz A (2000) Emerald mineralisation in Colombia: fluid chemistry and the role of brine mixing. Miner Deposita 35: 699-713

Barth S (1993) Boron isotope variations in nature - a synthesis. Geol Rundschau 83: 640-651

565 Bohlke JK, Irwin JJ (1992) Laser microprobe analyses of Cl, Br, I and K in fluid inclusions -
566 implications for sources of salinity in some ancient hydrothermal fluids. Geochim
567 Cosmochim Acta 56: 203-225
568 Bowersox GW, Snee LW, Foord EF, Seal RRII (1991) Emeralds of the Panjshir Valley,
569 Afghanistan. Gems & Gemology 27: 26-39
570 Branquet Y, Laumonier B, Cheilletz A, Giuliani G (1999a) Emeralds in the Eastern Cordillera
571 of Colombia: Two tectonic settings for one mineralisation. Geology 27: 597-600
572 Branquet Y, Cheilletz A, Giuliani G, Laumonier B (1999b) Fluidized hydrothermal breccia in
573 dilatant faults during thrusting: the Colombian emerald deposits. In: McCaffrey KJW,
574 Lonergan L, Wilkinson JJ (eds) Fractures, fluid Flow and Mineralisation. Geological
575 Society, London, United Kingdom, Special Publications, 155, pp 183-195
576 Branquet Y, Giuliani G, Cheilletz A, Laumonier B (2015) Colombian emeralds and
577 evaporites: tectono-stratigraphic significance of a regional emerald-bearing evaporitic
578 breccia level. In: André-Mayer AS, Cathelineau M, Muchez Ph, Picard E, Sindern S (eds)
579 From source, transport and metal deposits to mineral resources in a sustainable world,
580 Proceedings of the 13th biennal meeting of the Society for Geology Applied to Mineral
581 Deposits, Nancy, France, pp 1291- 1294
582 Cheilletz A, Féraud G, Giuliani G, Rodriguez CT (1994) Time-pressure-temperature
583 formation of Colombian emerald: an $^{40}Ar/^{39}Ar$ laser-probe and fluid inclusion-
584 microthermometry contribution. Econ Geol 89: 361-380
585 Cheilletz A, Giuliani G, Branquet Y, Laumonier B, Sanchez AJM, Féraud G, Arhan T (1997)
586 Datation K-Ar et $^{40}Ar/^{39}Ar$ à 65 ± 3 Ma des gisements d'émeraude du district de Chivor-
587 Macanal: argument en faveur d'une déformation précoce dans la Cordillère Orientale de
588 Colombie. C R Acad Sci 324: 369-377
589 Ericksen GE (1983) The Chilean nitrate deposits. Am Sci 71: 366-374
590 Faryad SW (2002) Metamorphic conditions and fluid compositions of scapolite-bearing rocks
591 from the lapis lazuli deposit of Sare Sang, Afghanistan. J Petrol 43: 725-747
592 Feneyrol J (2012) Pétrologie, géochimie et genèse des gisements de tsavorite associés aux
593 gneiss et roches calco-silicatées graphiteux de Lemshuku et Namalulu (Tanzanie). Ph.D
594 Institut National Polytechnique de Lorraine, Vandœuvre-lès-Nancy, France
595 Feneyrol J, Giuliani G, Ohnenstetter D, Le Goff E, Malisa PJ, Saul M (2010)
596 Lithostratigraphic and structural controls of tsavorite deposits at Lemshuku, Merelani area,
597 Tanzania. Contrôles lithostratigraphique et structural des gisements de tsavorite de
598 Lemshuku, région de Merelani, Tanzanie. C R Acad Sci 342: 778-785

599 Feneyrol J, Ohnenstetter D, Giuliani G, Fallick AE, Rollion-Bard Cl, Robert JL, Malisa E
600 (2012) Evidence of evaporites in the genesis of the vanadian grossular tsavorite deposit in
601 Namalulu, Tanzania. Can Mineral 50: 745-769
602 Feneyrol J, Giuliani G, Ohnenstetter D, Fallick AE, Martelat JM, Monié P, Dubessy C,
603 Rollion-Bard Cl, Le Goff E, Malisa E, Rakotondrazafy AFM, Pardieu V, Kahn T, Ichang'i,
604 D, Venance E, Voarintsoa NR, Ranatsenho M, Simonet C, Omito E, Nyamai C, Saul M
605 (2013) Worldwide tsavorite deposits: new aspects and perspectives. Ore Geol Rev 53: 1-25
606 Fritz H, Abdelsalam M, Ali KA, Bingen B, Collins AS, Fowler AR, Ghebread W,
607 Hauzenberger CA, Johnson PR, Kusky TM, Macey P, Muhongo S, Stern RJ, Viola G
608 (2013) Orogen styles in the East Africa region: a review of the Neoproterozoic to
609 Cambrian tectonic evolution. J Afr Earth Sci 86: 65-106
610 Garnier V, Ohnenstetter D, Giuliani G (2004) L'aspidolite fluorée: rôle des évaporites dans la
611 genèse des marbres de Nangimali (Azad-Kashmir, Pakistan). C R Acad Sci 336: 1245-
612 1253
613 Garnier V, Maluski H, Giuliani G, Ohnenstetter D, Schwarz D (2006) Ar-Ar and U-Pb ages
614 of marble-hosted ruby deposits from central and southeast Asia. Can J Earth Sci 43: 509-
615 532
616 Garnier V, Giuliani G, Ohnenstetter D, Fallick AE, Dubessy J, Banks D, Hoàng Quang V,
617 Lhomme Th, Maluski H, Pêcher A, Bakhsh KA, Pham Van L, Phan Trong T, Schwarz D
618 (2008) Marble-hosted ruby deposits from central and Southeast Asia: towards a new
619 genetic model. Ore Geol Rev 34: 169-191
620 Giuliani G, Cheilletz A, Dubessy J, Rodriguez CT (1993a) Emerald deposits from Colombia:
621 chemical composition of fluid inclusions and origin. In: Nägele u. Obermiller (eds)
622 Proceedings of the 8th biennal IAGOD symposium, Ottawa, Canada. pp 159-168
623 Giuliani G, Cheilletz A, Sheppard SMF, Arboleda C (1993b) Geochemistry and origin of the
624 emerald deposits of Colombia. In: Hach-Ali F, Torres L and Gervilla F (eds) Current
625 research in geology applied to ore deposits, Proceedings of the 2nd biennal meeting of the
626 Society for Geology Applied to Mineral Deposits, Granada, Spain, pp 105-108
627 Giuliani G, Cheilletz A, Arboleda C, Rueda F, Carillo V, Baker J. (1995) An evaporitic origin
628 of the parent brines of Colombian emeralds: fluid inclusion and sulfur isotopic evidence. Eur
629 J Mineral 7: 151-165
630 Giuliani G, France-Lanord C, Zimmermann JL, Cheilletz, A, Arboleda C, Charoy B, Coget P,
631 Fontan F, Giard D (1997) Composition of fluids, δD of channel H_2O and $\delta^{18}O$ of lattice

oxygen in beryls: genetic implications for Brazilian, Colombian and Afghanistani emerald deposits. Intern Geol Rev 39: 400-424

Giuliani G, France-Lanord Ch, Cheilletz A, Coget P, Branquet Y, Laumonier B (2000) Sulfate reduction by organic matter in Colombian emerald deposits: chemical and stable isotope (C, O, H) evidence. Econ Geol 95: 1129-1153

Giuliani G, Dubessy J, Banks D, Hoang Quang V, Lhomme T, Pironon J, Garnier V, Phan Trong T, Pham Van L, Ohnenstetter D, Schwarz D (2003) CO_2-H_2S-COS-S_8-AlO(OH)-bearing fluid inclusions in ruby from marble-hosted deposits in Luc Yen area, North Vietnam. Chem Geol 194: 167-185

Giuliani G, Groat L, Ohnenstetter D, Fallick AE, Feneyrol J (2014a) The geology of gems and their geographic origin. In: Raeside ER (ed) Geology of Gem Deposits, Mineralogical Association of Canada, Short Course Series 44, Tucson, USA, pp 113-134

Giuliani G, Ohnenstetter D, Fallick AE, Groat L, Fagan J (2014b) The geology and genesis of gem corundum deposits In: Raeside ER (ed) Geology of Gem Deposits, Mineralogical Association of Canada, Short Course Series 44, Tucson, USA, pp 29-112

Giuliani G, Dubessy J, Banks D, Lhomme Th, Ohnenstetter D (2015a) Fluid inclusions in ruby from Asian marble deposits: genetic implications. Eur J Mineral 27: 393-404

Giuliani G, Ohnenstetter D, Rollion Cl, Feneyrol J, Martelat JE, Omito E, Ichang'i D, Nyamai Ch, Wamunyu A (2015b) The boron isotopic composition of tourmaline from tsavorite deposits in the Neoproterozoic Mozambique metamorphic belt, with a special focus on the mining districts in Kenya. In: André-Mayer AS, Cathelineau M, Muchez Ph, Picard E, Sindern S (eds) From source, transport and metal deposits to mineral resources in a sustainable world, Proceedings of the 13th biennal meeting of the Society for Geology Applied to Mineral Deposits, Nancy, France, pp 1319-1322

Groat L.A. (2014) Geology of Gem Deposits. Mineralogical Association of Canada Short Course series 44, Raeside R. (ed), Tucson Arizona, USA

Hubbard MS, Grew ES, Hodges KV, Yates MG, Pertsev NN (1999) Neogene cooling and exhumation of upper-amphibolite-facies 'whiteschists' in the southwest Pamir Mountains, Tajikistan. Tectonophysics 305: 325-337

Hughes R.W. (1997) Ruby and Sapphire, RW Hughes publishing, Boulder, USA

Kazmi AH, Snee LW (1989) Emeralds of Pakistan, Van Nostrand Reinhold, New York, USA

Kozlowski A, Metz P, Jaramillo HAE (1988) Emeralds from Sodomondoco, Colombia: chemical composition, fluid inclusion and origin. Neues Jahrbuch Miner Abh 59: 23-49

665 Kulke HG (1974) Die lapis-lazuli Sar-e-Sang (Badakhshan): geologie, entstehung,
666 kulturgeschete und bergau. Afghanistan Journal: 43-56
667 Kulke HG, Schreyer W (1973) Kyanite-talc schist from Sar e Sang, Afghanistan. Earth Planet
668 Sci Lett 18: 324-328
669 Lacassagne V, Besseda C, Florian P, Bouvet S, Olliver B, Coutures JP, Massiot D (2002)
670 Structure of high temperature NaF-AlF_3-Al_2O_3 melts: a multinuclear NMR study. J Phys
671 Chem 106: 1862-1868
672 Laumonier B, Branquet Y, Cheilletz A, Giuliani G, Rueda F (1996) Les gisements
673 d'émeraude de Muzo et de Coscuez (ouest de la Cordillère Orientale de Colombie) sont des
674 duplex formés pendant une phase de tectonique en chevauchement à la limite Eocène-
675 Oligocène. C R Acad Sci 320: 1171-1178
676 Machel HG, Krouse HR, Sassen R (1995) Products and distinguishing criteria of bacterial and
677 thermochemical sulphate reduction. Appl Geochem 10: 373-389
678 Mattauer M, Matte Ph, Jolivet JL, (1999) A 3D model of the India-Asia collision at plate
679 scale: C R Acad Sci 328: 499-508
680 Olivier B (2006) The geology and petrology of the Merelani tanzanite deposit, NE Tanzania.
681 Ph.D University of Stellenbosch, South Africa
682 Ottaway TL, Wicks FJ, Bryndzia LT, Kyser TK, Spooner ETC (1994) Formation of the Muzo
683 hydrothermal emerald deposit in Colombia. Nature 369: 552-554
684 Pêcher A, Giuliani G, Garnier V, Maluski H, Kausar AB, Malik RM, Muntaz HR (2002)
685 Geology and Geochemistry of the Nangimali ruby deposit area, Nanga-Parbat Himalaya
686 (Azad Kashmir, Pakistan). J Asian Earth Sci 21: 265-282
687 Pokrovski GS, Dubrovinsky LS (2011) The S^{3-} ion is stable in geological fluids at elevated
688 temperatures and pressures. Science 331: 1052-1054
689 Pokrovski GS, Dubessy J (2014) Stability and abundance of the trisulfur radical ion S^{3-} in
690 hydrothermal fluids. Earth Planet Sci Lett 411: 298-309
691 Polovov IB, Vasin BD, Abakumov AV, Rebrin OI, Chernyshov MV, Volkovich VA, Griffiths
692 TR (2007) Thermodynamics of the formation of vanadium (II) complexes in chloride
693 melts. In*:* Mantz RA, Hagiwara M, Trulove HC, De Long H, Stafford GR, Fox D (eds)
694 "Molten Salts", ECS Transactions" 3, Issue 35, The Electrochemical Society, Pennington,
695 pp 589-597
696 Reinen D, Lindner GG (1999) The nature of chalcogen colour centres in ultramarine-type
697 solids. Chem Soc Rev 28: 75-84

698 Roedder E (1963) Studies of fluid inclusions II: freezing data and their interpretation. Econ
699 Geol 58: 163-211
700 Sabot B, Cheilletz A, De Donato P, Banks D, Levresse D, Barrès O (2000) Afghan emeralds
701 face Colombian cousins. Chron Rech Min 541: 111-114
702 Samson I, Anderson A, Marshall D (2003) Fluid inclusions: Analysis and interpretation.
703 Mineralogical Association of Canada, Short Course series 32, Raeside R. (ed), Vancouver,
704 British Columbia, Canada
705 Schreyer W, Abraham K (1976) Three-stage metamorphic history of a whiteschist from Sar e
706 Sang, Afghanistan, as part of a former evaporite deposit. Contrib Mineral Petrol 59: 111-
707 130
708 Tapponnier P, Mattauer M, Proust F, Cassaigneau Ch (1981) Mesozoic ophiolites, sutures,
709 and large-scale tectonic movements in Afghanistan. Earth Planet Sci Lett 52: 355-371
710 Tenczer V, Hauzenberger C, Fritz H, Hoinkes G, Muhongo S, Klötzli U (2013) Crustal age
711 domains and metamorphic reworking of the deep crust in Northern-Central Tanzania: a
712 U/Pb zircon and monazite age study. Mineral Petrol 107: 679-707
713 Truche L, Bazarkina EF, Barré G, Thomassot E, Berger G, Dubessy J, Robert P (2014) The
714 role of S^{3-} ion in thermochemical sulphate reduction: geological and geochemical
715 implications. Earth Planet Sci Lett 396: 190-200
716 Van Hinsberg VJ, Henry DJ, Marschall HR (2011) Tourmaline: an indicator of its host-
717 environment. Can Mineral 49: 1-16
718 Vapnik YE, Moroz I (2001) Fluid inclusions in Panjshir emerald (Afghanistan). In: Noronha
719 F, Dória A, Guedes A (eds), XVI European current research on fluid inclusions, (ECROFI),
720 Porto, Portugal, Faculdade de Ciências do Porto, Memoria 7, pp 451-454
721 Vasin BD, Polovov IB, Volkovich VA, Griffiths TR, Berezin AV (2004) Coordination state
722 of vanadium in chloride melts: an electronic absorption spectroscopy study. In: Mantz RA,
723 Trulove HC, De Long H, Stafford GR, Hagiwara M, Costa DA (eds) "Molten Salts XIV",
724 Proceedings of the International symposium, Electrochemical Society, 2004-24, New
725 Jersey, USA, pp 261-268
726 Warren JK (2006) Evaporites: Sediments, Resources and Hydrocarbons. Springer, Berlin,
727 Germany
728 Williams AE, McKibben MA (1989) A brine interface in the Salton Sea Geothermal system,
729 California: fluid, geochemical and isotopic characteristics. Geochim Cosmochim Acta 53:
730 1905-1920

731 Wilson WE, Saul JM, Pardieu V, Hughes RW (2009) The Merelani tanzanite mines. Mineral
732 Record 40: 347-408

733 Wood SA (1992) Theoretical prediction of speciation and solubility of beryllium in
734 hydrothermal solution to 300°C at saturated vapour pressure: application to
735 berttrandite/phenakite deposits. Ore Geol Rev 7: 249-278

736 Yardley WB, Cleverley JS (2013) The role of metamorphic fluids in the formation of ore
737 deposits. In: Jenkin GRT, Lusty PAJ, McDonald I, Smith MP, Boyce AJ, Wilkinson JJ
738 (eds), Ore Deposits in an Evolving Earth. Geol Soc London, Special Publications 393. doi:
739 10.1144/SP393.5

740 Yardley WB, Bodnar RJ (2014) Fluids in the continental crust. Geochem Persp Lett 3: 1-127

741

742

743

744 **Figure captions**

745 **Figure 1.** Metamorphic gems. A- Crystal of emerald on pyrite, Chivor mines, eastern
746 emerald belt, Colombia, 3.9x2.6 cm. Collection MultiAxes. B- Association of emerald and
747 quartz, Muzo mines, western emerald belt, Colombia. C- Emerald crystals on quartz and
748 adularia, Panjshir Valley, Afghanistan, 6.6x4.4 cm. Specimen Fine Art Mineral. D- Ruby
749 crystal associated with flakes of phlogopite in a marble matrix, Minh Tien mine, Luc Yen
750 mining district, Vietnam, 2x1 cm. E- Nodule, rough and cut of tsavorite from the Tsavolite
751 mine, Mangare mining district, Voi region, Kenya, diameter of the nodule (on the left) ~ 3.5
752 cm. F- Association lazurite, carbonate and pyrite from Sar-e-Sang mines, Afghanistan,
753 8.3x6.2 cm, Specimen Crystal Classics. G- Gem crystal of tsavorite (2 cm across) embedded
754 in a graphitic gangue with calcite (white), Merelani mines, Arusha district, Tanzania. H- Blue
755 zoisite, variety tanzanite, Merelani, Arusha district, Tanzania, 8.7x5x3 cm. Collection Marcus
756 Budil. Photos: A to C, F to H, L.-D. Bayle/le Règne Minéral. Photo D: G. Giuliani. Photo E:
757 V. Pardieu/GIA.

758 **Figure 2.** Colombian emerald mines (modified from Branquet et al. 2015). A- Simplified
759 geological map of the Colombian Eastern Cordillera with the location of the main emerald
760 deposits. Inset is location of Figure 2B. B- Geological map of the Chivor area. All emerald
761 and gypsum deposits and occurrences are hosted within the upper Guavio Formation.

762 **Figure 3.** Geological features of Cr-V-bearing metamorphic gems formed during the
763 metamorphism of rocks (black shale-carbonate-sandstone with evaporite intercalations) from

carbonate platform successions. Be: beryllium; Al: aluminium; Si: silica; Ca: calcium; Cr: chromium; V: vanadium. Colombian emerald deposits: a: Mg-limestone; b: emerald-bearing calcareous C-rich BS; c: sandstone; d: pyritic nodules in siliceous BS; e: siliceous BS. Ruby in marble from central and south-east Asia: f: quartzite; g: amphibolite; h: mica-bearing marble; i: pyrite-bearing marble; j: calc-schist and garnet-biotite micaschist; k: ruby-anhydrite-bearing yellow Mg-marble; l: white dolomite and/or calcite marbles. Tsavorite in graphitic gneiss and calc-silicates from Tanzania: m: biotite-kyanite gneiss; n: graphitic gneiss; o: tsavorite-bearing nodules in graphitic gneiss and calc-silicate rocks with anhydrite-gypsum veinlets or lenses; p: calc-silicate rocks; q: kyanite-graphite gneiss; r: dolomitic marble with anhydrite levels (modified from Giuliani et al. 2014b).

Figure 4. A- Geological cross-section through the Chivor emerald deposits, eastern emerald belt (from Branquet et al. 2015). B- South-eastern field view of the cross-section. C- Chivor Klein pit. Upper contact of the main breccia level (in black) with albitites (1). The transport of clasts of albitite (2) within the breccia is marked by tails. D- Oriente deposit. Polygenic breccia formed by clasts of albitite (Ab) and black shales (Bs), cemented by pyrite, carbonates and albite. E- Oriente deposit. Carbonate (Cb) -pyrite (Py) -emerald-bearing veins crosscutting albitite (Ab) showing some remnants of black shale (Bs). The greyish tracks parallels to the carbonate veins are residues of dust not cleaned by the water jet in the mine. Photos B to D: Y. Branquet and Photo E: G. Giuliani.

Figure 5. Geological map of the Tequendama and Quipama mines, Muzo mining district, western emerald belt. U1 through U4 represent the different tectonic units. The cross-section A-B is drawn on figure 6. Modified from Laumonier et al. (1996).

Figure 6. Cross-section of the Tequendama mine located at the northern part of the Muzo emerald mining district (A-B section as shown on Figure 5). The deposit is linked to tear faults and associated thrusts which are marked by the overlying of the siliceous black shales by the carbonated ones. The thrust planes are underlined by a hydrothermal breccia (called "cenicero" by the miners) and hydraulic fracturing. The fluid circulation induced intense albitisation, carbonatisation and pyritisation of the surrounding black shales (modified from Branquet et al. 1999b).

Figure 7. Hydraulic fracturing breccia of black shale located in the tear fault of Coscuez mine, western Colombian emerald belt. Photo: Y. Branquet.

795 **Figure 8.** Location of the Panjshir emerald and Sar-e-Sang lapis-lazuli deposits in
796 Afghanistan, and ruby-hosted marble from central and south-east Asia. The main tectonic
797 structures and blocks are reported from Mattauer et al. (1999): CF: Chaman fault, GF:
798 Gaoligong fault, SF: Sagain fault, RRF: Red River fault, HK: Hindu Kush, K: Kohistan, P:
799 Pamir.

800 **Figure 9.** (A) Tectonic map of Kenya and Tanzania (modified after Fritz et al. 2013) with
801 the localities of the main tsavorite and tanzanite deposits. (B) Tectonic map of Madagascar
802 (modified after Fritz et al. 2013) with the locality of the tsavorite deposits. (C) Geological
803 sketch map of SE Kenya and NE Tanzania (modified after Tenczer et al. 2013) with the
804 localities of the tsavorite and tanzanite. ANS: Arabian Nubian Shield; EG: Eastern Granulite;
805 WG: Western Granulite.

806 **Figure 10.** Tsavorite mineralisation from the Neoproterozoic Metamorphic Mozambique
807 Belt in southeastern Kenya and northeastern Tanzania. A- Calc-silicates band (Csb) hosting
808 diopside (Di) nodules in the graphitic gneiss (Grg) from the Davis Mine, Lualenyi mining
809 district, Mgama ridge, Kenya. B- Nodule of anhydrite (Anh) and green grossular (Grs-
810 tsavorite) presenting a 'chicken-wire' texture in a matrix composed of quartz (Qtz) and calcite
811 (Cal). The nodules are at the contact with the graphitic gneiss (Grg) which have
812 accumulations of graphite (Gr). Classic mine, eastern part of the Mgama ridge, Kenya. C-
813 Tsavorite is hosted by meta-evaporitic horizons intercalated in the graphitic gneiss (Grg). The
814 anhydrite-bearing level (Anh) is formed by nodules showing enterolithic textures and the
815 anhydrite-alunite (Sulph) level. D- Tsavorite-bearing nodule from the Komolo mine, south of
816 Arusha, northeastern Tanzania. The nodule is zoned and the mineral assemblages are, from
817 the centre to the periphery: (i) V- green grossular in the centre (Grs); (ii) the first rim (R1) is
818 formed predominantly by anhydrite (Anh) + gypsum (Gp), quartz and minor V-titanite, V-
819 zoisite and small crystals of tsavorite; (iii) the second rim (R2) contains anhydrite (Anh) +
820 gypsum, clay and minor V-free zoisite; and (iv) the external zone is the graphitic gneiss (Grg)
821 with quartz, plagioclase, K-feldspar, V-kyanite, V-muscovite, V-rutile, graphite (Gr), F-rich
822 phlogopite (Phl) and minor calcite and jarosite. Photographs A to C: G. Giuliani; D: J.
823 Feneyrol.

824 **Figure 11.** SEM images showing the presence of sulphate and salt inclusions in the gems
825 or associated minerals. A- Ruby (Crn) in equilibrium with dolomite (Dol) formed from the
826 reaction of spinel (Sp) with calcite. Spinel is a pre-ruby phase which contains high Cr (up to
827 19 wt. %) and Zn contents (10 wt. %). Spinel is associated with anhydrite (Anh). Hunza

828 Valley, Pakistan. B- The nodule of tsavorite shows remnants of barite (Brt) substituted by
829 diopside (Di), titanite (Ttn) and tsavorite (Ts), Mine of Nadan 1, Voi region, Kenya. C- Halite
830 crystal (NaCl) in ruby (Crd). Mine of Jegdalek (Afghanistan). D- Crystals of anhydrite (Anh)
831 associated with phlogopite (Phl) included in a ruby (Crd) from the Nangimali deposit, Azad
832 Kashmir, Pakistan. E- Mixtures of salts (Ca-Na-K-[Cl] and sylvite (KCl) found in ruby (Crd)
833 from the deposits of Luc Yen, Vietnam. F- Anhydrite (Anh) inclusion associated with F-
834 tremolite (F-Tr) and dolomite (Dol) in marble, Namalulu tsavorite deposit, south of Arusha,
835 northern Tanzania. G- Tainolite (Tnl) associated with calcite (Cal) in a dolomite (Dol) lens
836 from the Namalulu tsavorite deposit.

837 **Figure 12.** Parental fluids of emerald, ruby and tsavorite. A- Tabular fluid inclusion
838 trapped by a Colombian emerald (Chivor mine, eastern emerald belt). The primary cavity
839 contains a liquid (L), vapour (V), two cubes of halite (H) and a minute crystal of calcite (Cal).
840 B- Fluid inclusion in a Colombian emerald showing three cubes of halite (H), the liquid phase
841 (L), the contracted vapour phase (V), a minute black phase (S) and a thin rim of liquid carbon
842 dioxide (L_1) rim visible at the bottom part of the vapour phase. C- Multiphase primary fluid
843 inclusions trapped by an emerald from the Panjshir Valley (Afghanistan). The cavity contains
844 a vapour (V) and liquid (L) phases, a cube of halite (H), usually a primary and rounded salt of
845 sylvite (Syl) and aggregates of several unidentified anisotropic grains (S). D- Primary
846 polycrystalline fluid inclusions trapped by the Mogok ruby in marble from Myanmar. The
847 cavity contains different solids which are mixtures of carbonates, with Ca-Na-Al cations such
848 as calcite (Ca), dawsonite (Dw), shortite (Sh), and apatite (Ap), fluorite (Fl), halite (H),
849 graphite and a CO_2-H_2S-bearing fluid phase (CO_2). E- Primary multiphase H_2S-dominated FI
850 (liquid [L_{H2S}] + vapour [V_{H2S}]) with native sulphur (S_8), phengite (Phg) and calcite (Cal) in a
851 tsavorite from Merelani. Photos: G. Giuliani.

852 **Figure 13.** Origin of salinity in the emerald and quartz-related brines from Colombia and
853 Afghanistan. A- Analyses of the fluid inclusions from both emerald and quartz show a wide
854 range of Na/Br and Cl/Br molar ratios that are much greater than those of primary halite and
855 indicate a substantial loss of Br, typical of recrystallised halite for both emerald deposits. B-
856 Log(I/Cl) versus Log(Br/Cl) molar ratios of Afghan and Colombian fluid inclusions which are
857 depleted in both Br and I, indicative of evaporites contribution to the fluids in emerald and
858 quartz. They are compared with composition of fluids where evaporites are known to be
859 involved such as for the Salton Sea geothermal brines (Williams and McKibben 1989) and
860 Hansonburg (Bohlke and Irwin 1992).

Figure 14. Diagram log (K/Na) molar ratio versus 1/T (°K) showing the evolution of the fluids associated with Colombian and Afghan emeralds relatively to crustal fluids including bittern brines, brines derived by dissolution of evaporites, and magmatic fluids (modified from Yardley and Bodnar 2014). Sedimentary formation brines deviate significantly from the K-feldspar-albite equilibrium as well as for Afghan and Colombian brines which are associated with a huge albitisation of their host-rock with the complete consumption of K-feldspar from respectively, the schist and black shale.

Figure 15. Boron isotopic composition of tourmalines associated with tsavorite from Kenya, Tanzania and Madagascar. The $\delta^{11}B$ (‰) of tourmalines clearly involves continental evaporitic material (Feneyrol 2012). The boron isotopic ranges of other Kenyan tourmalines associated with different rocks from the tsavorite-bearing metasedimentary series are reported for comparison (Giuliani et al. 2015b). The different boxes representative of different geological environments are from Barth (1993) and van Hinsberg et al. (2011).

Figure 16. The formation of metamorphic tsavorite-bearing nodules in a closed metamorphic system (from Feneyrol et al. 2013). A- The sedimentary nodule is initially an anhydrite concretion within the silica-rich shales. These shales contained V(-Cr)-rich clays and organic matter. B- At the beginning of the prograde metamorphism, the host shales turned into schists, and V(-Cr)-rich clays and organic matter transformed into respectively V(-Cr)-rich micas and graphite. For the formation of tsavorite, Si and Al came from the schist, V and Cr from the clays and/or organic matter, and Ca from the anhydrite following the equation: $3CaSO_4 + 2Al^{3+} + 3SiO_2 + 6H_2O \rightarrow Ca_3Al_2(SiO_4)_3 + 6O_2 + 3H_2S + 6H^+$.
H_2S is trapped by the fluid inclusion cavities in tsavorite. The sulphur is expelled into the schist to form pyrite. C- At the end of the prograde metamorphism, most of the anhydrite has been replaced by tsavorite which is also present as small crystals scattered in the evaporitic rims of the nodule. Pyrite, graphite and V(-Cr)-poor mica are the main minerals present in the surrounding gneiss.

Table caption

Table 1. Reconstruction composition of emerald-related fluids from the Panjshir deposits, Afghanistan (this work). For comparison are reported the composition of the fluids associated with Colombian emeralds (Banks et al. 2000).

Table

country	deposit	mineral	salinity (wt% eq. NaCl)	Na	K	Li	F (ppm)	Cl	Br	SO_4	I	Na/K (m)	Na/Br (m)	Cl/Br (m)	Na/Li (m)	Cl/SO_4 (m)	og(Br/Cl (m)	log(I/Cl) (m)
AFGHANISTAN																		
	Kendjt	quartz	34	103.711	25.250	171	118	206.310	44.2	147	0.29	6.98	8152.12	10520.63	182.55	3792.17	-4.02	-6.40
	Kendjt	"	34	107.729	26.800	180	115	206.310	36.4	143	0.31	6.83	10286.9	12780.53	180.24	3905.72	-4.11	-6.38
	Kendjt	emerald	34	78.205	34.062	207	670	206.310	41.4	4310	0.49	3.9	6563.65	11233.31	114.02	129.63	-4.05	-6.18
	Butizor	"	34	97.257	22.573	220	nd	206.310	20	1058	0.8	7.32	16928.4	23296.37	133.67	528.13	-4.37	-5.97
	Gujari	"	34	72.325	30.322	261	nd	206.310	39.8	1331	0.41	4.05	6311.74	11680.32	83.68	419.57	-4.07	-6.25
	Shigar	"	34	71.969	29.692	245	nd	206.310	41.2	824	0.52	4.12	6065.24	11279.71	88.73	677.63	-4.05	-6.16
COLOMBIA*																		
	Yacopi	emerald	38	100.376	22.585		nr	224.007	80.2	6491	4.5	7.56	4347.85	6294.79		93.45	-3.80	-5.25
	Coscuez	"	38	130.946	5795	944	nr	230.082	36.7	463	0.3	0.04	12395	14128.97	41.86	1345.61	-4.15	-6.44
	Cincho	"	37	94.823	18.813	1261	nr	224.306	39.7	166	1.9	8.57	8297.40	12733.39	22.69	3658.9	-4.10	-5.63
	Palo Aranado	"	40	122.677	8829	1165	nr	242.43	55.5	232	0.68	0.02	7678.72	9844.35	31.77	2829.55	-3.99	-6.11
	Oriente	"	38	116.142	5888	430	nr	230.202	27.4	352	0.36	0.03	14725.1	18934.43	81.5	1770.86	-4.28	-6.36
	Klein	"	40	98.923	10.248	1959	nr	240.698	51.0	1966	2.61	16.41	6738.23	10636.44	15.24	331.52	-4.03	-5.52
	Yacopi	quartz	40	94.019	19.556		nr	240.815	328.1	1567	0.9	8.17	995.47	1654.14		416.13	-3.22	-5.98
	Coscuez	"	35	54.590	11.622	2031	nr	211.091	100.6	1189	0.2	7.99	1885.10	4728.96	8.11	480.74	-3.67	-6.58
	Coscuez	"	41	106.484	14.833		nr	248.415	118.4	238	0.9	12.20	3124.29	4728.46		2826.31	-3.67	-5.99
	Coscuez	"	42	92.542	10.467	2212	nr	254.132	65.8	658	3	15.03	4885.76	8704.17	12.62	1045.81	-3.94	-5.48
	Cincho	"	39	63.557	11.567	4322	nr	230.481	99.0		1.6	9.34	2230.22	5246.79	4.44		-3.72	-5.71
	Cincho	"	41	103.599			nr	247.813	390	558	5		922.80	1432.03		1202.56	-3.16	-5.25
	Pava	"	41	110.776	5449	432	nr	227.371	150.7	24	2.7	0.03	2553.59	3400.29	77.37	25653.2	-3.53	-5.48
	Oriente	"	31	76.239	12.389		nr	188.233	87.7	997	3.1	10.46	3019.93	4837.15		511.23	-3.68	-5.34
	Klein	"	31	68.344	8796	2549	nr	183.208	42.8		1.5	0.01	5547.22	9647.05	8.09		-3.98	-5.64
	Guali		40	78.554	17.415	2090	nr	242.078	23.8	614	2.2	7.67	11466	22923.04	11.34	1067.59	-4.36	-5.60

nd: not detected; nr: not reported because measured at the limit of detection (~ 1ppm); * Banks et al. (2000)

Figure

Click here to download Figure Fig. 1.jpg

Figure

Click here to download Figure Fig. 2.jpg

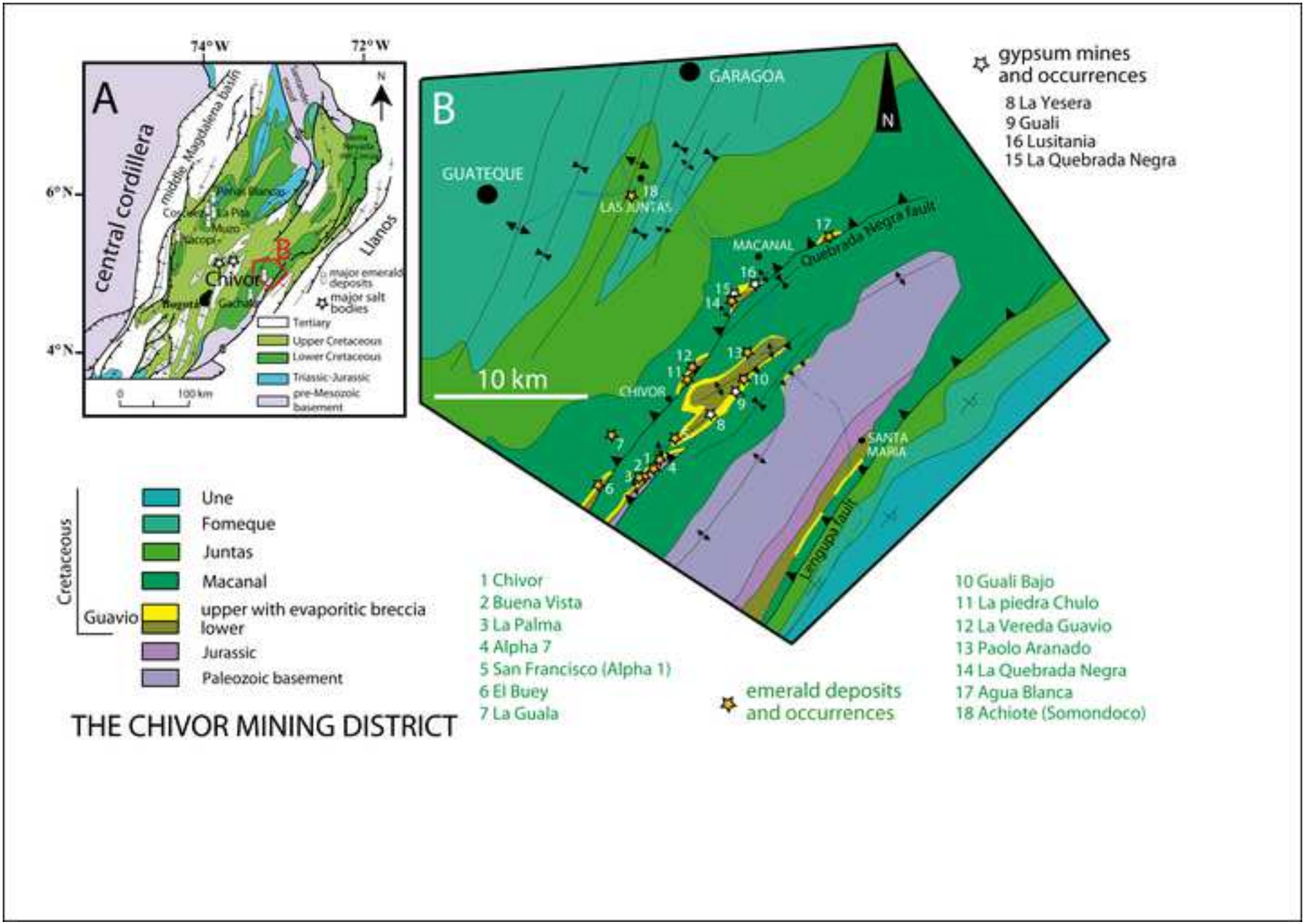

Figure

Click here to download Figure Fig. 3.jpg

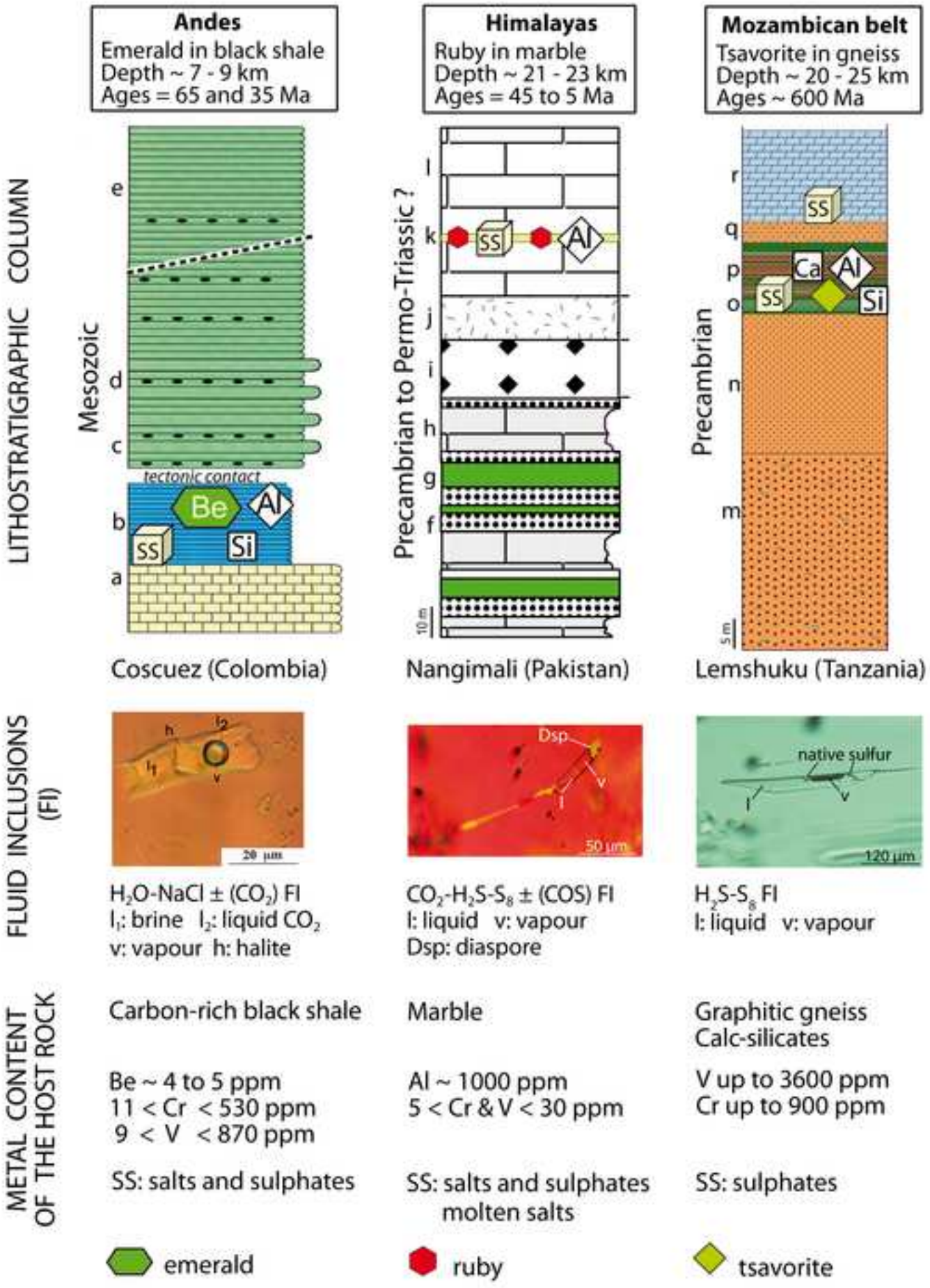

Figure

Click here to download Figure Fig. 4.jpg

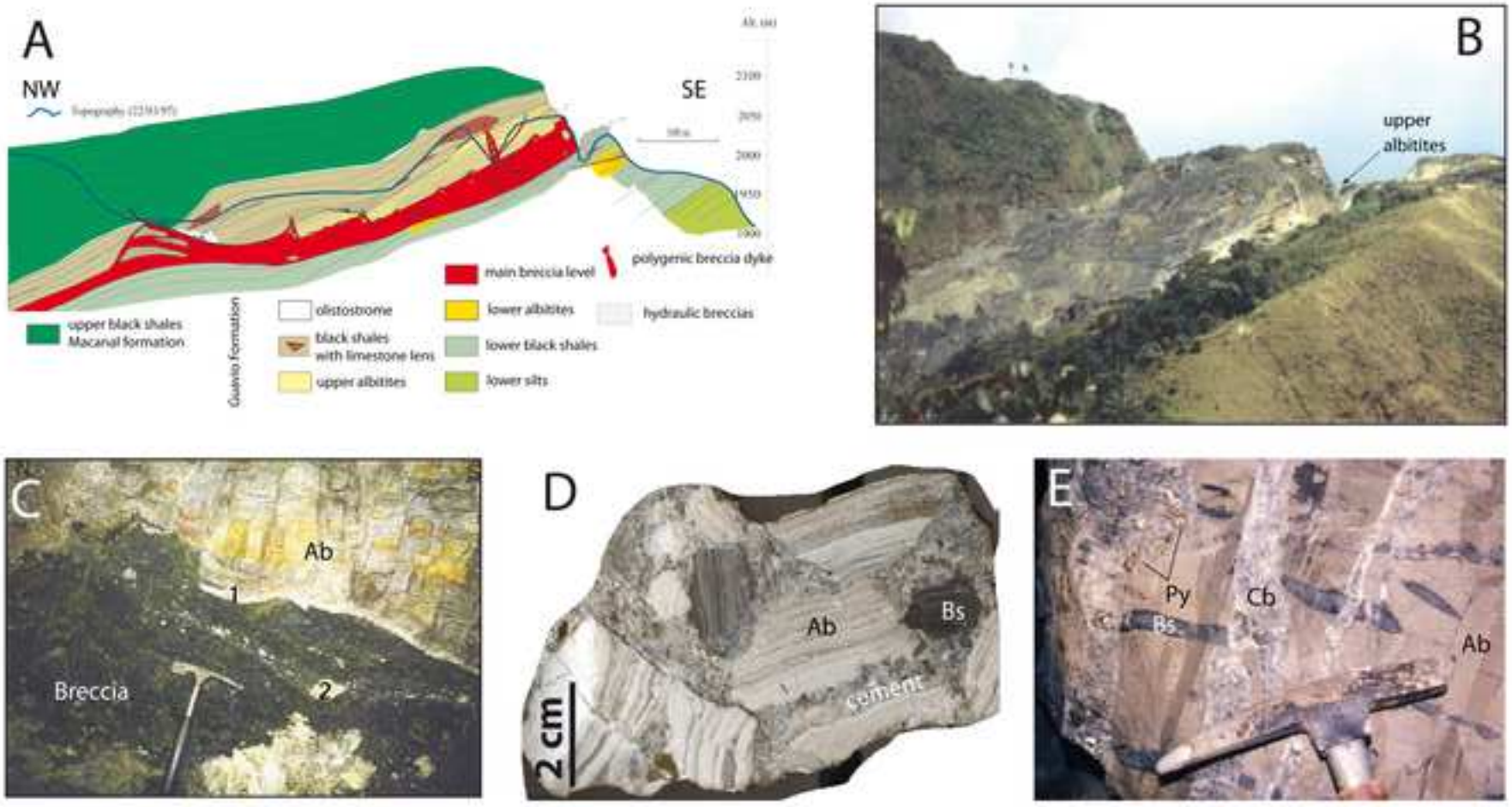

Figure

Click here to download Figure Fig. 5.jpg

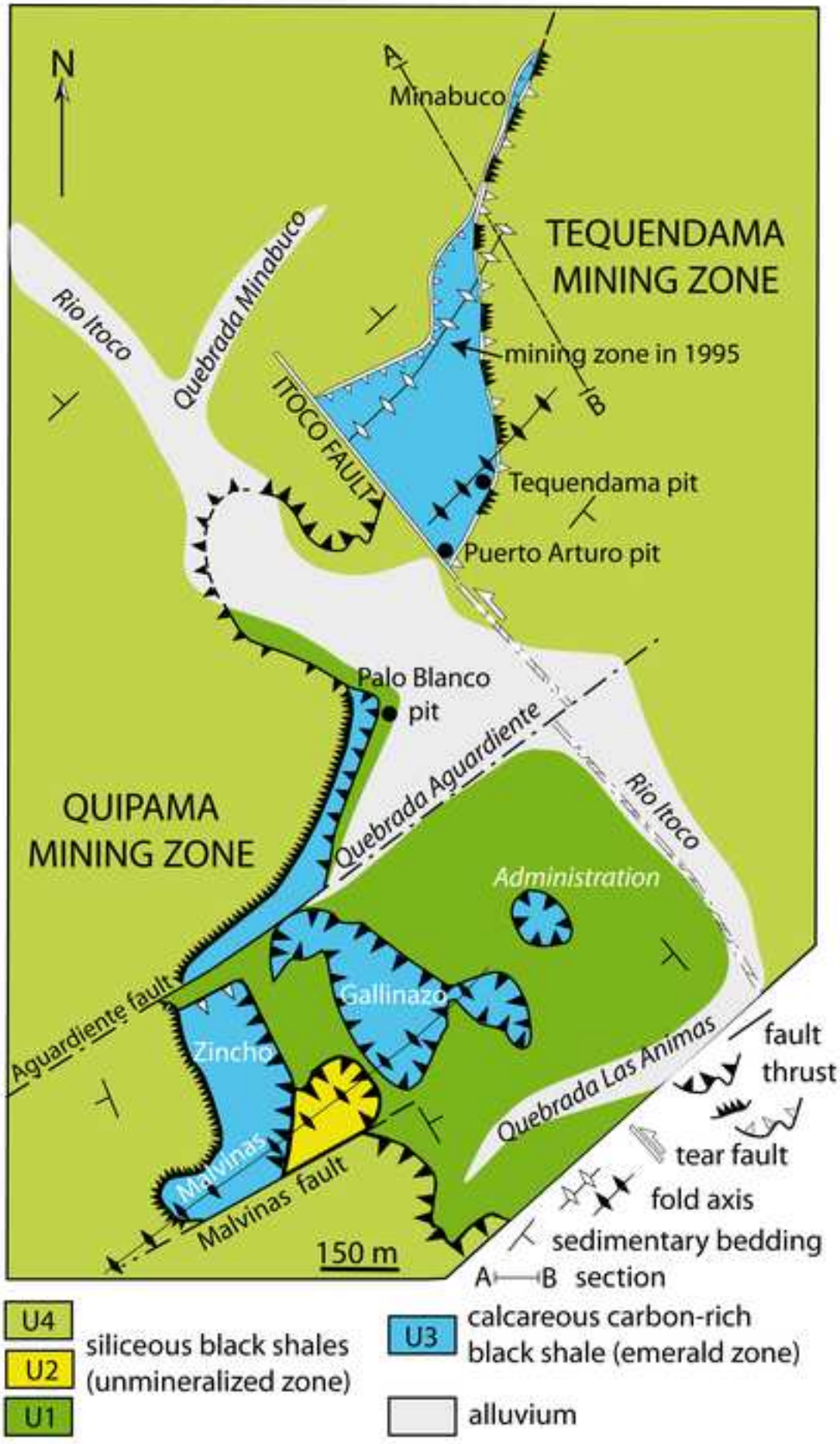

Figure

Click here to download Figure Fig. 6.jpg

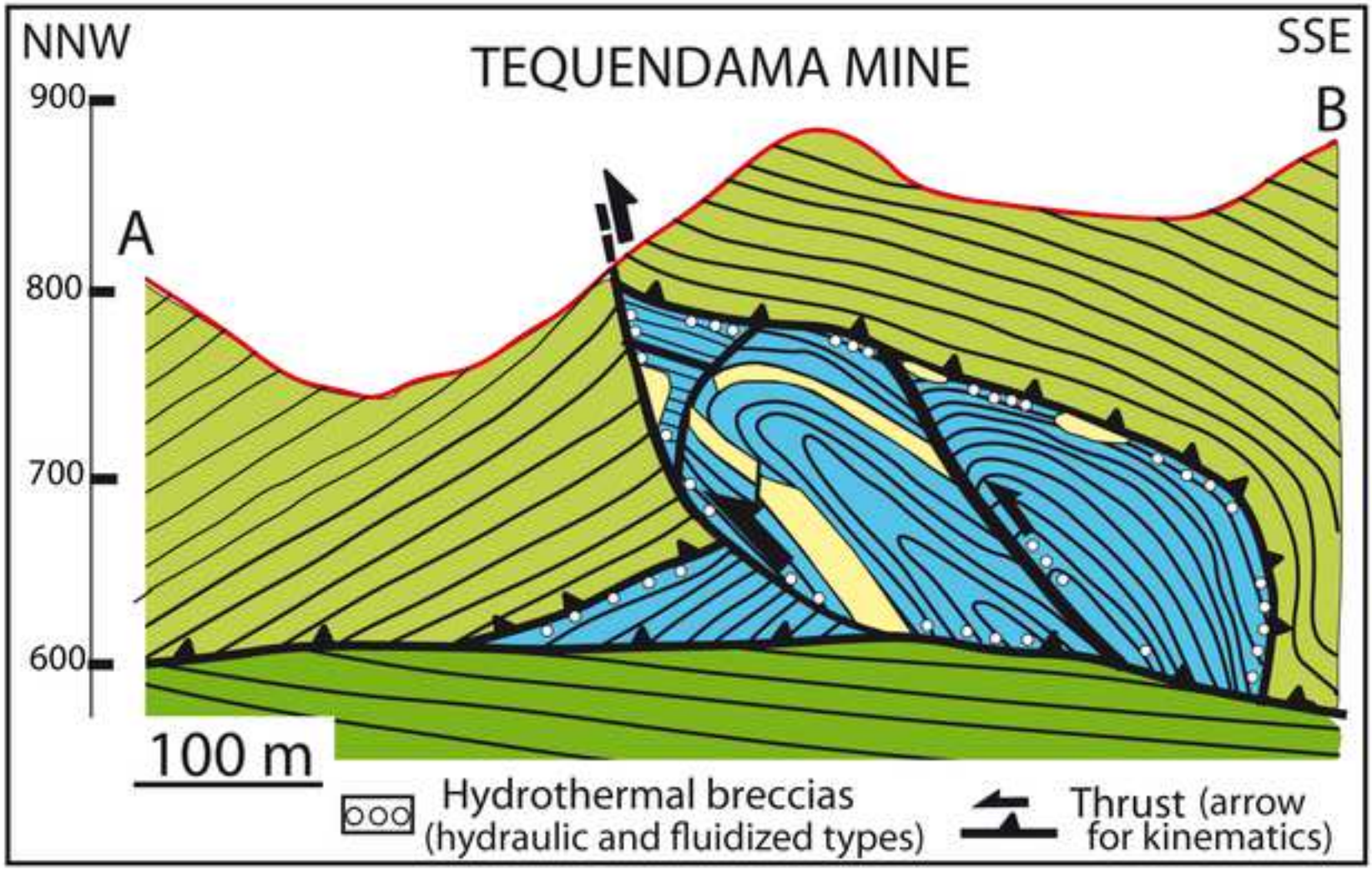

siliceous black shales (permeability barrier)

carbonated black shale (fluid-saturated rock mass)

albitites

Figure

Click here to download Figure Fig. 7.jpg

Figure

Click here to download Figure Fig. 8.jpg

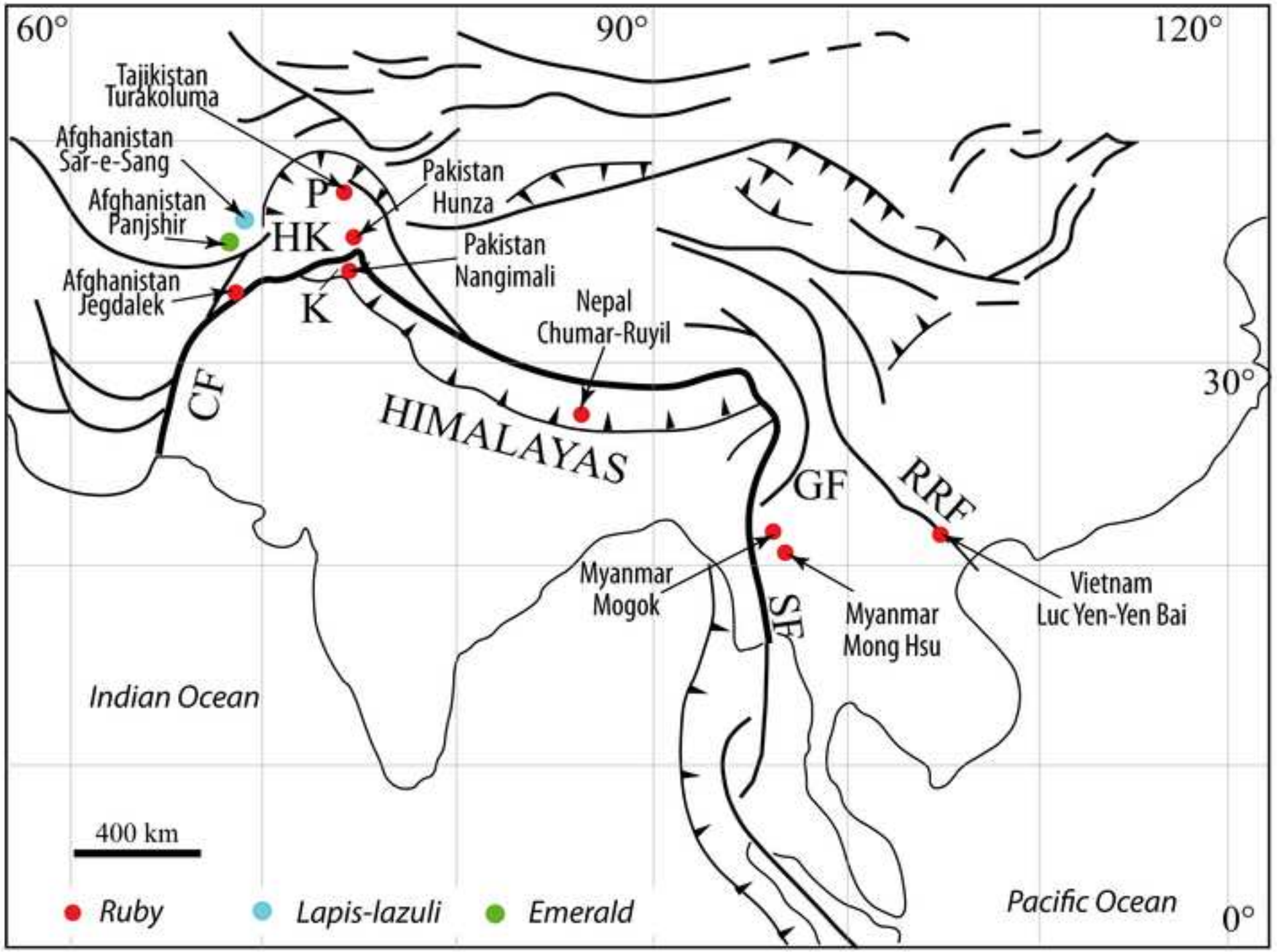

Figure

Click here to download Figure Fig. 9.jpg

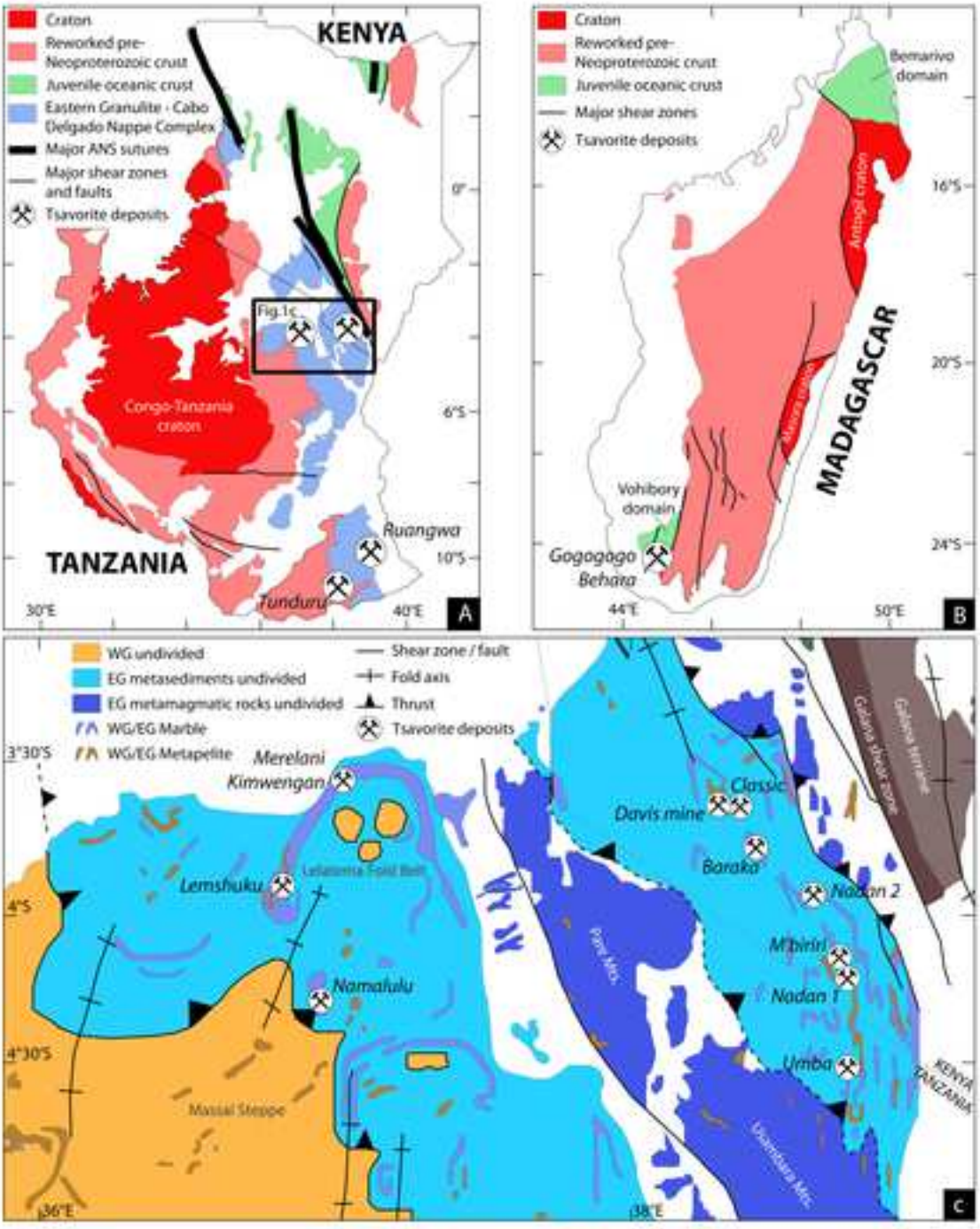

Figure

Click here to download Figure Fig.10. ai.jpg

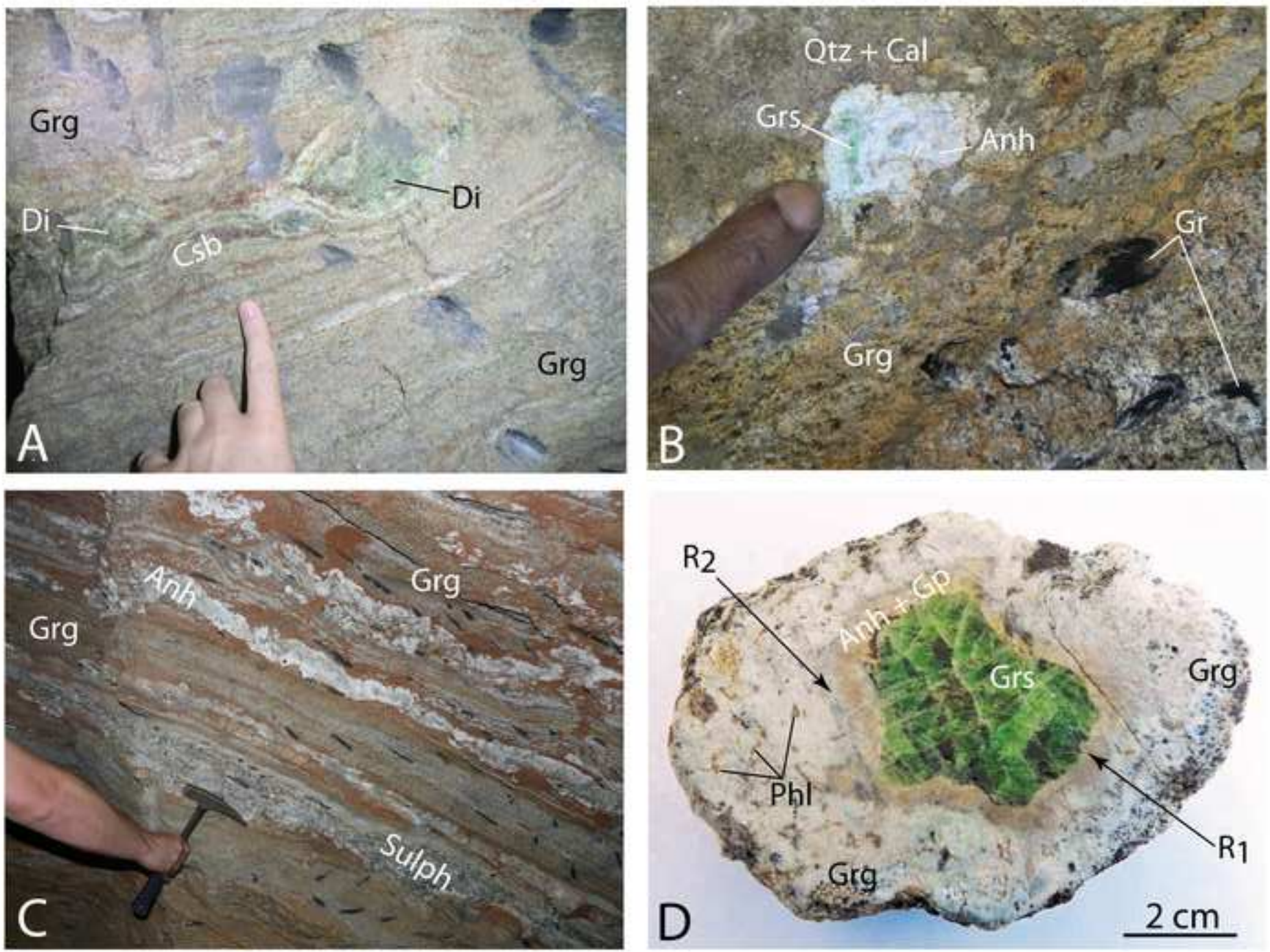

Figure

Click here to download Figure Fig. 11. .jpg

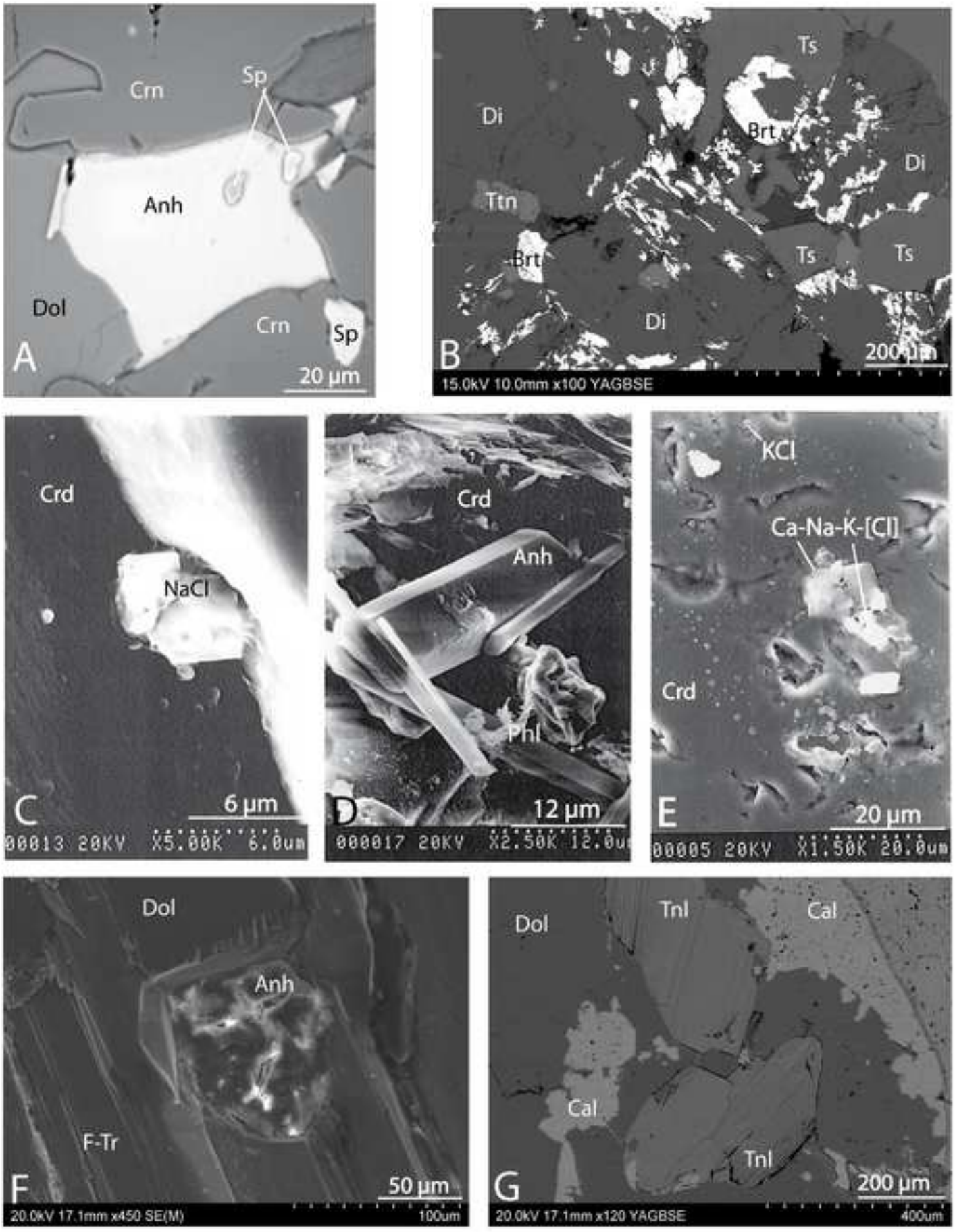

Figure

Click here to download Figure Fig. 12.jpg

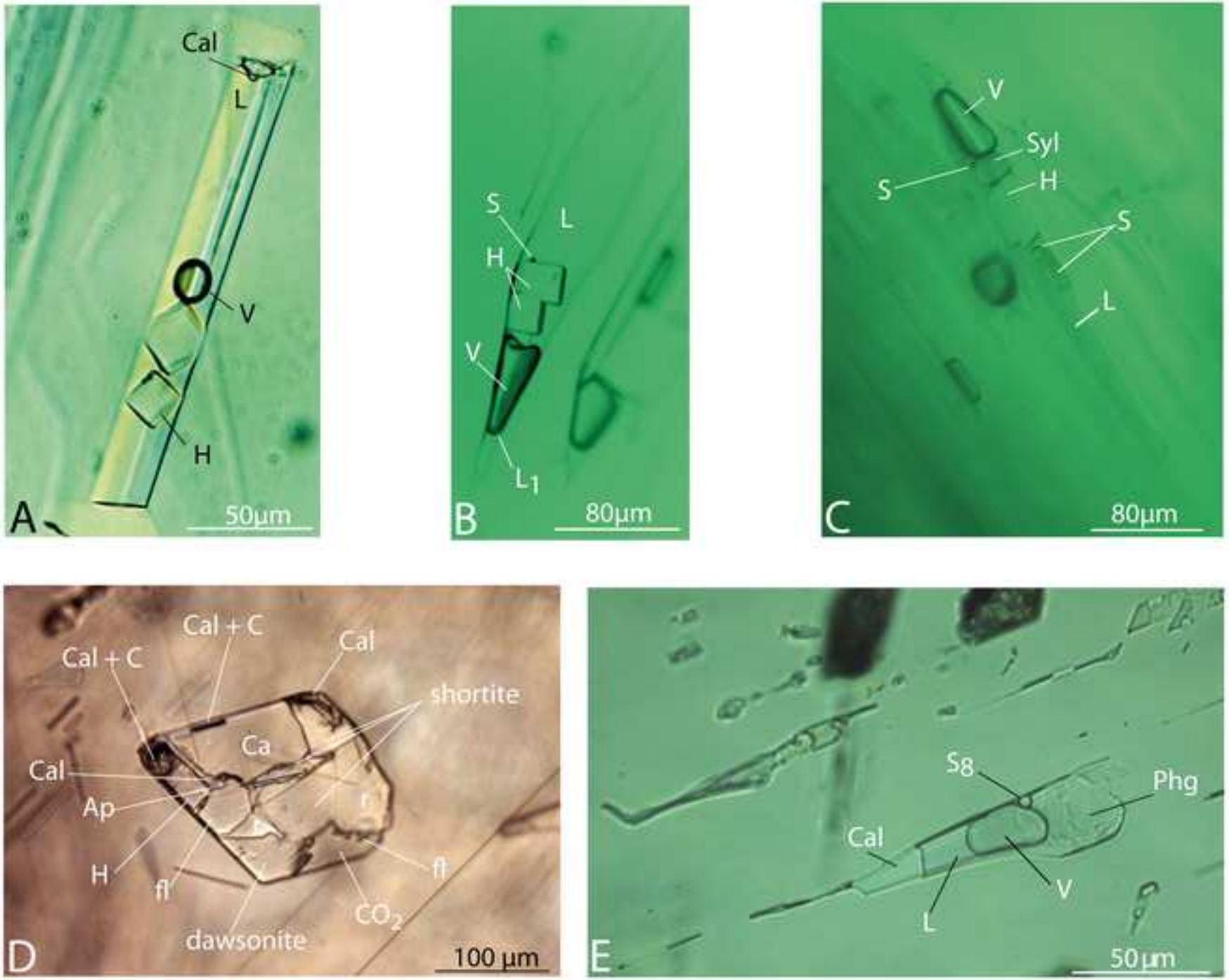

Figure

Click here to download Figure Fig. 13.jpg

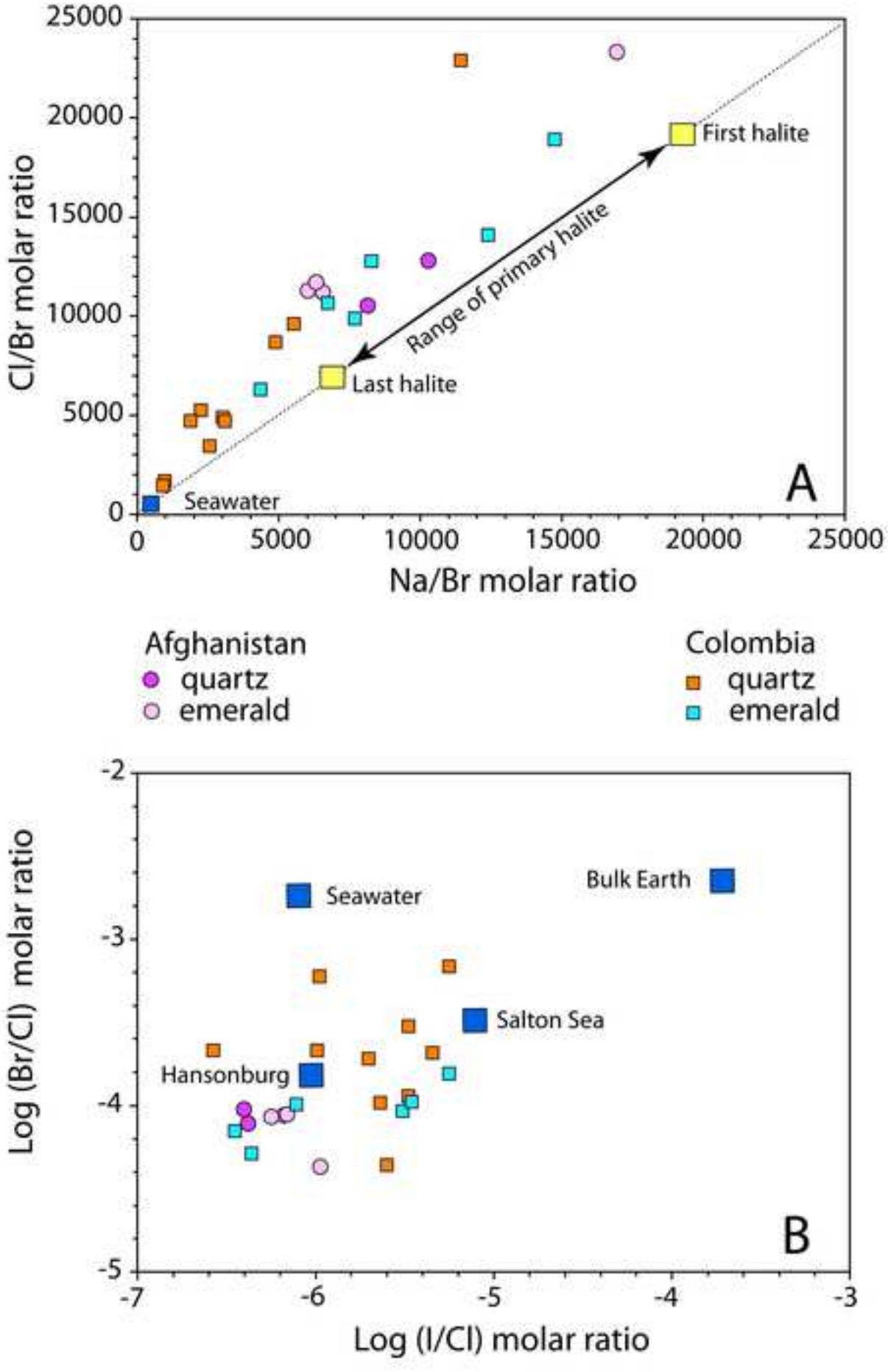

Figure

Click here to download Figure Fig. 14.jpg

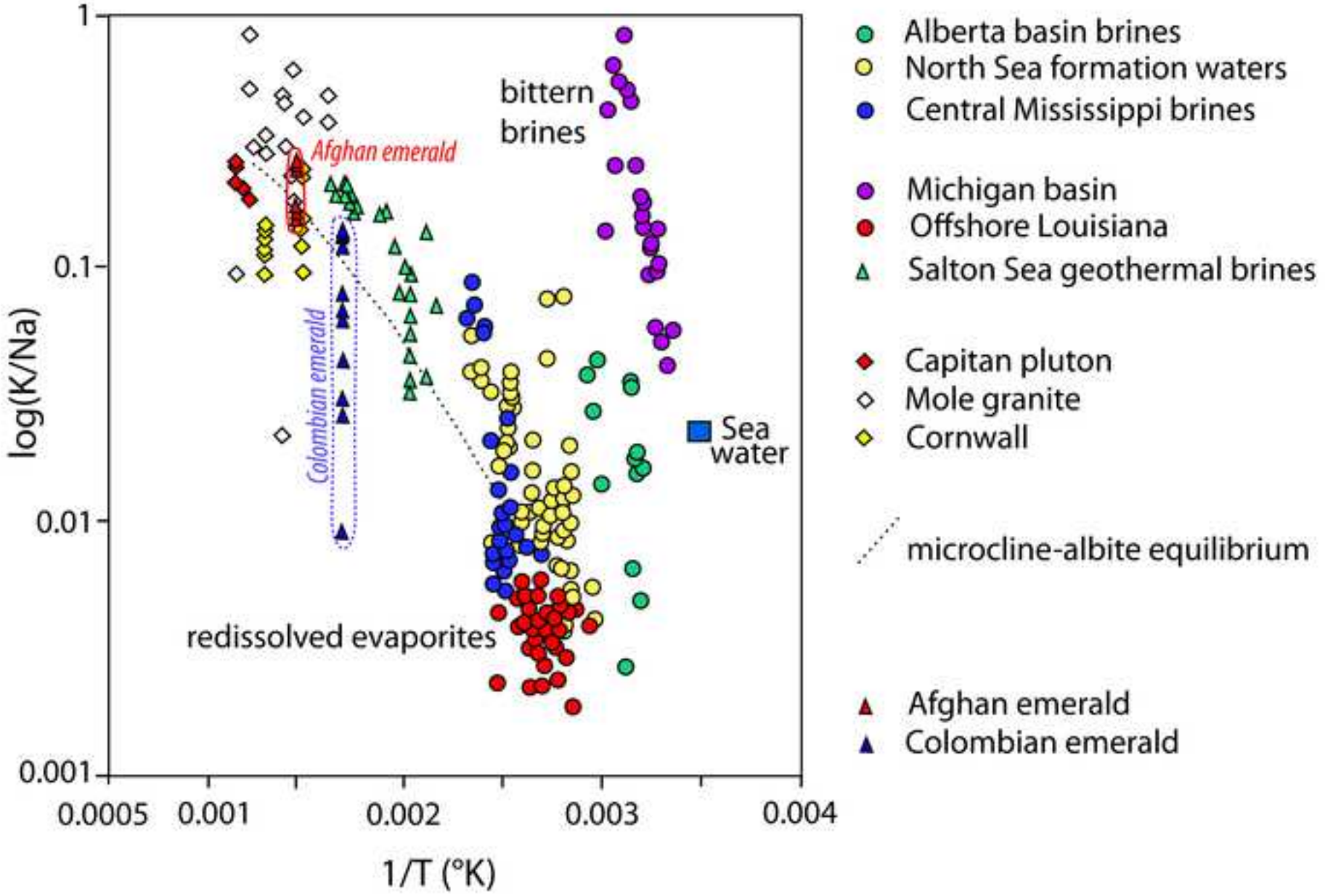

Figure

Click here to download Figure Fig. 15 Bore Tourmalines.jpg

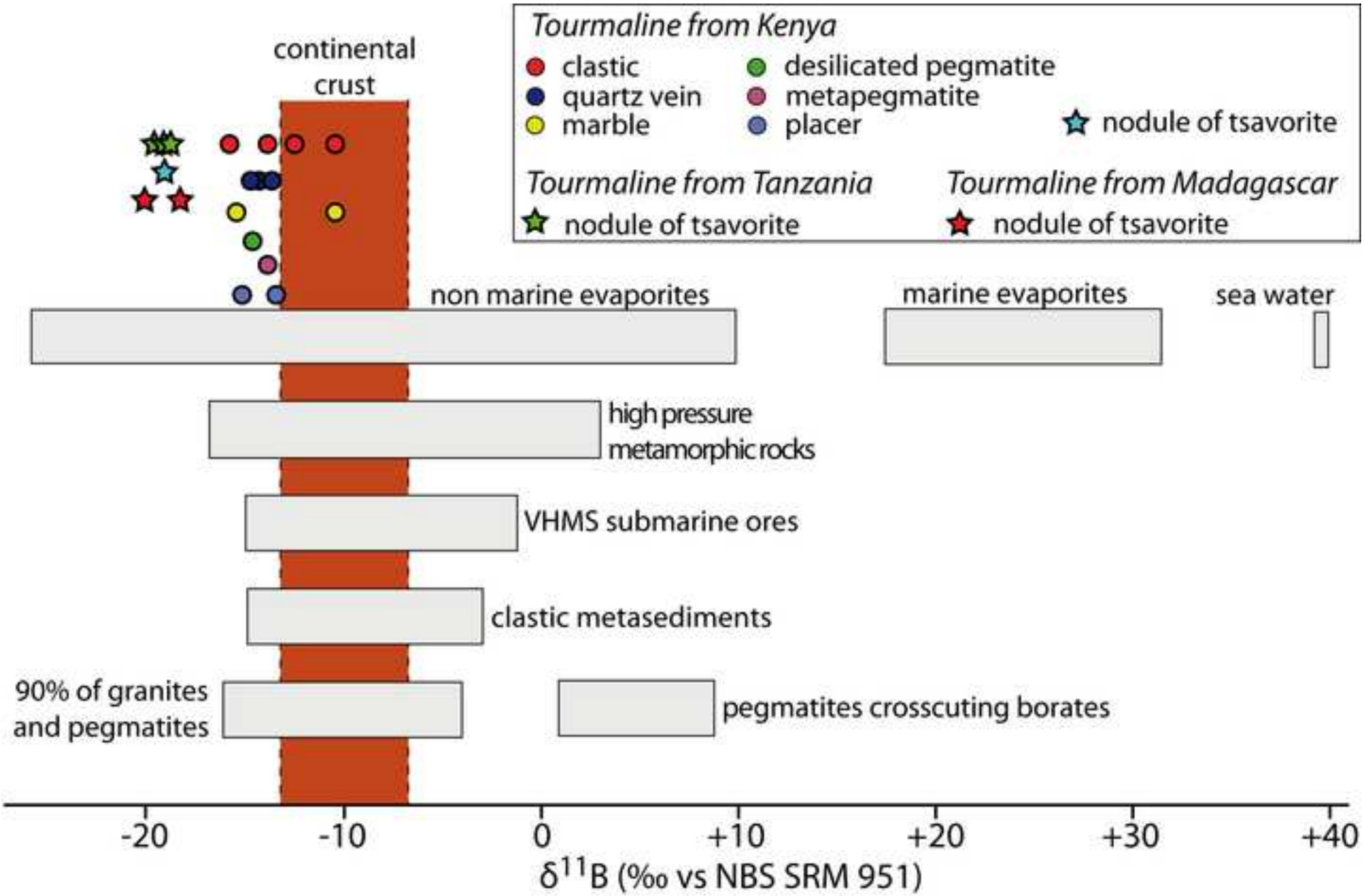

Figure

Click here to download Figure Fig.16.jpg